Journal of Hydrology 598 (2021) 126220

Contents lists available at ScienceDirect

Journal of Hydrology

journal homepage: www.elsevier.com/locate/jhydrol

Research papers

The proportion of jet flow and on-wall flow and its effects on soil loss and plunge pool morphology during gully headcut erosion

Mingming Guo [a,b], Yibao Lou [c], Zhuoxin Chen [c], Wenlong Wang [b,c,*], Lanqian Feng [b], Xingyi Zhang [a]

[a] Key Laboratory of Mollisols Agroecology, Northeast Institute of Geography and Agroecology, Chinese Academy of Sciences, Harbin, Heilongjiang, 150081, PR China
[b] State Key Laboratory of Soil Erosion and Dryland Farming on the Loess Plateau, Institute of Soil and Water Conservation, Chinese Academy of Sciences and Ministry of Water Resources, Yangling, Shaanxi, 712100, China
[c] State Key Laboratory of Soil Erosion and Dryland Farming on the Loess Plateau, Institute of Water and Soil Conservation, Northwest A&F University, Yangling, Shaanxi, 712100, China

ARTICLE INFO

This manuscript was handled by Renato Morbidelli, Editor-in-Chief, with the assistance of Corrado Corradini, Associate Editor

Keywords:
Gully erosion
Plunge pool erosion
Headcut retreat
Morphology evolution
Energy consumption

ABSTRACT

Gully headcut erosion is recognized as the primary process of gully erosion and is the main contributor to sediment yield of gully erosion. However, the proportion of jet flow and on-wall flow induced by headcut and its effects on soil loss and plunge pool morphology are still unclear. A simulated flow-scouring experiment was conducted to explore the proportion of jet flow and on-wall flow and their contributions to soil loss and the effect of on-wall flow erosion on plunge pool morphology under different flow discharge (q_0 = 3.0–7.2 m^3 h^{-1}) and headwall height (H_0 = 0.3–1.2 m) conditions. Our results showed that jet flow and on-wall flow accounted 15.7% − 22.6% and 77.4% − 84.3% of total flow volume upstream headcut, respectively. Jet flow, on-wall flow and their interaction contributed 53.5%, 34.9% and 11.6% of total soil loss amount, respectively. Furthermore, H_0 exhibited greater effect on soil loss caused by jet flow and its interaction with on-wall flow, but the soil loss caused by on-wall was mainly controlled by q_0. The width and depth of plunge pool logarithmically increased with scouring time, and the q_0 and H_0 significantly affected the development of plunge pool morphology. On-wall flow reduced plunge pool depth by 27.8%–71.4%, and it weakened plunge pool width by 24.3%−57.3% only under H_0 of 0.3–0.9 m, but for H_0 of 1.2 m and q_0 of >4.8 m^3 h^{-1}, it improved the plunge pool width by 7.5%. The energy consumption of jet flow showed the closest relationship with plunge pool morphology. The concentrated flow upstream gully head exhibited the stronger effect on plunge pool morphology than H_0. This study is helpful to deepen the understanding of gully erosion mechanism and provide scientific reference for the design of gully erosion prevention and control measures.

1. Introduction

Soil erosion is a worldwide ecological environment problem and an important manifestation of land degradation. Gully erosion can contribute 10% − 94% of total sediment yield caused by water erosion (Poesen et al., 2003). Inevitably, gully erosion also can cause lots of serious damages and adverse influences, such as devouring the high-quality fertile farmlands, damaging infrastructures, improving the hydrological and sediment connectivity of the basin, and increasing the sediment transport ratio of the basin (Heckmann et al., 2018). It is noteworthy that gully headcut erosion has been recognized as the primary process of gully erosion, including headcut migration and plunge pool erosion, and was usually the main contributor to sediment yield of gully erosion (Oostwoud-Wijdenes et al., 2000; Oostwoud-Wijdenes and Bryan, 2001; Gómez-Gutiérrez et al., 2014). Some previous studies also suggested that gully headcut erosion is a critical scientific issue that needs to be strengthened in the field of soil erosion (e.g., Vanmaercke et al., 2016; Zhang, 2020).

Gully headcut erosion involves a variety of sub-processes of staggered superposition and interaction, mainly including tension fissure development, pore water pressure change, on-wall flow erosion, plunge pool erosion, and mass failure. These sub-processes play important roles

* Corresponding author at: State Key Laboratory of Soil Erosion and Dryland Farming on the Loess Plateau, Institute of Water and Soil Conservation, Northwest A&F University, Yangling, Shaanxi, 712100, China.
E-mail address: nwafu_wwl@163.com (W. Wang).

https://doi.org/10.1016/j.jhydrol.2021.126220
Received 13 December 2020; Received in revised form 27 February 2021; Accepted 15 March 2021
Available online 23 March 2021

in controlling the development of headcut erosion and contribute to soil loss and morphology at different degrees (Collison, 2001; Wells et al., 2009a; Su et al., 2014; Vanmaercke et al., 2016). However, most of the studies on these sub-processes are in the stage of theoretical analysis and statistical analysis of monitoring data, and their influencing mechanism is still rarely explored. Gully headcut erosion is affected by many factors, such as topography, land use, climate, soil, vegetation and so on. With respect of topography, most of studies focused on the relationship between slope S and catchment area A ($S = a{\cdot}A^b$), and some progress also has been made in the change in value of a and b with influencing factors (Wu & Cheng, 2005; Claudio et al., 2006; Cheng et al., 2006; Torri and Poesen, 2014). Plant coverage is a common vegetation parameter that is used to evaluate the influence of vegetation on sheet soil erosion. However, in fact, the influence of vegetation on headcut erosion mainly depends on root architecture and its density and distribution in soil layers (Vannoppen et al., 2015; Vanmaercke et al., 2016). At present, there is still some controversy about the influence of land use on gully erosion initiation (Vandekerckhove et al., 2001). It is highly recommended that more attention should be paid to the role of root system in controlling headcut erosion when studying the influence of land use and vegetation on gully erosion (Vanmaercke et al., 2016; Guo et al., 2019). Soil properties, such as soil physical and chemical properties, vertical joints, soluble mineral content, geotechnical properties, soil layer structures, also have been proven to significantly affect gully head migration, gully wall collapse and the topographic criticality of gully erosion initiation (Vanwalleghem et al., 2003; Sanchis et al., 2008; Torri and Poesen, 2014). Climate is also an important factor affecting gully erosion. Previous studies mainly focused on the critical precipitation and runoff initiating gully erosion (Ionita, 2006; Rodzik et al., 2009; Moeyersons et al., 2015), but the great difference in critical values under different erosion environment conditions. Especially, in the high latitude cold cool area, the gully headcut erosion is affected by the interaction of freeze–thaw cycle, snowmelt and rainfall (Wu et al., 2008; Liu et al., 2013; Li et al., 2016; (Xu et al., 2019), and thus the activation mechanism is more complex. From the point view of gully erosion study method, most of the current studies were conducted by remote sensing image interpretation, real-time monitoring and Meta-analysis based on published literature data to analyze the gully erosion changes during a given temporal-spatial scales. As a result, we just obtained the changes in gully erosion amount and morphological parameters in a certain historical period, and the change is the result of the interaction of various factors (Guo et al., 2019). However, the influencing mechanism of these factors during headcut erosion is not yet known and the gully erosion process under real ground conditions also involves a lot of influencing factors and is very complicated. Therefore, it is urgent to carry out factors-controlled experiments to clarify their influencing mechanism and contributions to gully erosion.

Although soil erosion due to head cut migration can contribute the most of soil loss, soil loss as a result of head cut migration and plunge pool erosion was not explicitly addressed in some frequently used soil erosion models. Since 1990s, some researchers began to try to develop some empirical headcut erosion models considering soil properties, jet flow energy, jet shear stress and headwall collapse or some theoretical models based on mechanic principle, mass conservation, energy conservation laws (e.g., De Ploey, 1989; Robinson & Hanson, 1994; Temple and Moore, 1997; Alonso et al., 2002; Prasad & Römkens, 2003; Rengers & Tucker, 2014), whereas these models were not popularly applied in previous studies. The main reasons are that: 1) these models are available only under some limited conditions (Alonso et al., 2002), and 2) these models highly generalized these complex sub-processes of headcut erosion, leading to the idealization of these real sub-processes (Hanson et al., 2001). As we know, the formation of headcut is the main cause of the complicated erosion processes. The concentrated flow would be separated into jet flow and on-wall flow when it passes the edge of headwall, and then the jet flow dominates the plunge pool erosion and the on-wall flow causes the headwall erosion (involving water erosion and mass failure) (Zhang et al., 2016; Guo et al., 2019; Shi et al., 2020). The water erosion and headwall collapse induced by on-wall flow would affect the plunge pool erosion process. However, the proportions of on-wall flow and jet flow to total flow volume and their response to flow discharge and headwall height, the contribution of the interaction of jet flow and on-wall flow to total soil loss, and the influence of on-wall flow erosion on the development of plunge pool morphology were not clear. More importantly, the lack of solutions to these problems is detrimental to the revelation of the hydrodynamic mechanism of gully headcut erosion and the establishment of a process-based gully erosion model.

Therefore, we hypothesized that the proportions of jet flow and on-wall flow at the edge of headwall were affected by flow discharge upstream from drainage area and headwall height and further influence soil loss of gully heads and the development of plunge pool morphology. Therefore, we designed three types of controlled-experiments including jet flow experiment (on-wall flow was separated), on-wall flow experiment (jet flow was separated), and the mixed flow experiment (the flow was not separated) under different gully head height and flow discharge conditions to verify our hypothesis. The three specific objectives of this study are: 1) to clarify the proportions of on-wall flow and jet flow and its response to flow discharge and headwall height during gully headcut erosion, 2) to quantify the soil loss contributions of jet flow, on-wall flow and their interaction, and 3) to elucidate the influence of on-wall flow erosion and jet properties on the development of plunge pool morphology. This study is helpful to reveal the dynamic mechanism of gully erosion, establish gully erosion model, and provide scientific basis for the design and application of gully erosion prevention measures.

2. Materials and methods

2.1. Experimental flume set-up

This study was conducted in the Xifeng Soil and Water Conservation Experimental Station that is located in the Nanxiaohegou watershed (35°41′-35°44′N, 107°30–107°37′E), a typical gully-dominated watershed on the Loess Plateau, China. The experiment was conducted in a 6.5 m long and 1.5 m wide cement flume under simulated inflow scouring conditions (Fig. 1a). All experiments were completed from May to September in 2019 and from May to September in 2020. The cement flume consists of flat upstream area, vertical headwall and gully bed. The preliminary investigation showed that the widths and heights of gully-heads varied in ranges of 2–51 m and 3–37 m, respectively, and the range of breadth-height ratio is 0.75–5.67 (Che, 2012). Given the fact that the natural and real gully heads of such a large dimension cannot be simulated in soil flumes, we select to reduce the size but keep a reasonable breadth-height ratio. At last, the length of upstream area and gully bed is designed as 5.0 m and 1.5 m, respectively, and their slope was designed as 3°. The height of vertical gully headwall is set as 0.3, 0.6, 0.9 and 1.2 m, implying the breadth-height ratio (1.25–5.0) is within the real situation. Therefore, a total of four experimental flumes with four headwall heights were used in this study. The flume boundary was constructed in strict accordance with designed plot dimension using cement and bricks. A 0.6-m long and 0.5-m depth steady flow pool including the cobblestone (3–5 cm in diameter) and water energy dissipation structure with two cement baffles (0.3 m and 0.4 m height) (Guo et al., 2019; Shi et al., 2020) was set at the upstream top of the flume. The energy dissipation structure can almost consume the water energy, so that the water will gradually overflow from the steady flow pool and flow into the upstream area at almost zero energy when clear water was pumped into the steady flow pool (Fig. 1a). The flow discharge was controlled by two adjustable intake valves and monitored by an electromagnetic flowmeter. To facilitate the experiments and avoid the effects of natural rain, wind and sunshine on experimental schedule and operation, a moveable tent (length = 8.0 m, width = 3.0 m and height = 4.0 m) was installed around the plot (Fig. 1b).

The experiment was subjected to five upstream flow discharge (q) of

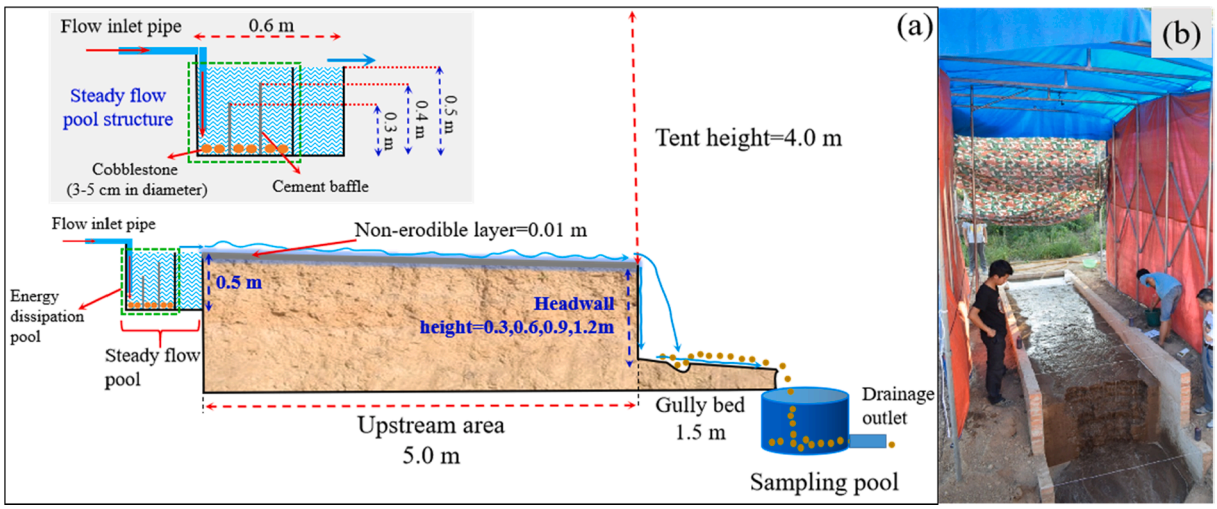

Fig. 1. Sketch of plots (a) and the experiment photo of mixed flow experiment (flow was not separated).

3.0, 3.6, 4.8, 6.0 and 7.2 $m^3\ h^{-1}$ which was designed as according to the rain intensity, drainage area upstream gully heads and rain duration in the Loess Plateau. The specific design is as following.

The average rainfall intensity (i) with different recurrence intervals could be calculated by Eq. (1) which was proposed by Zhang et al. (1983) according to a statistical analysis of 1710 typical rainstorm events in the study area.

$$i = \frac{5.09N^{0.379}}{(t+1.4)^{0.74}} \quad (1)$$

where i is the average rainfall intensity during t minutes, mm min^{-1}; N is the recurrence interval of heavy rainfall, yr; and t is the rainfall duration, min.

Jiao et al. (1999) concluded that the "A" type rainstorm with a rainfall duration of 30 to 180 min is the most common rainfall type on the Loess Plateau and can cause more serious soil erosion than other types of rainstorms. Thus, we selected the extreme case (180 min rainfall duration), and then the recurrence interval of rainstorms was selected as 1 ~ 10 years. The flow discharge calculated by Eq. (2) ranged from 3.12 to 7.49 $m^3\ h^{-1}$, and thus we selected the five levels (3.0, 3.6, 4.8, 6.0 and 7.2 $m^3\ h^{-1}$) from the calculated range.

$$q = \frac{60\lambda \cdot A \cdot i \cdot d}{w} \quad (2)$$

where q is the flow discharge, $m^3\ h^{-1}$; A is the drainage area upstream of the gully head (km^2), and ranges from 0.15 km^2 to 8.7 km^2 in this study region; w is the width of gully heads, km; d is the flume width (1.5 m); and λ is the runoff coefficient and is equal to 0.167 in this study region based on standard runoff plots (Li et al., 2006).

2.2. Soil bed preparation

The soil used in this study was chosen to represent textural composition and are commonly found in the gully-dominated watershed in the Loess Plateau. Before soil bed preparation, several basic soil properties were measured as a reference for soil filling operation. The mean clay, silt and sand content are 26.8%, 31.5% and 41.7%, respectively according to the USDA standard. The soil bulk density, organic matter content and stable infiltration rate are 1.35–1.55 g cm^{-3}, 0.52–1.12% and 0.21–0.63 mm min^{-1}, respectively. To ensure uniform soil bed conditions, all above-ground grass biomass, roots and debris were removed during the establishment of four soil flumes. Based on the investigated soil bulk density, the bulk density was controlled at 1.35 g cm^{-3} in 0–10 cm, 1.45 g cm^{-3} in 10–30 cm layer and 1.55 g cm^{-3} in >30 cm layers. The soil was back-filled in the plot in 10-cm thick layers. In the course of filling the flumes, each soil layer was tamped to ensure consistency, and the soil surface was raked between layers to promote cohesion between layers (Guo et al., 2019). The soil bulk density of gully bed was also controlled at 1.55 g cm^{-3}. The mass soil moisture was kept approximately at 15% during soil filling process, and thus the required soil amount in each 10-cm layer was calculated and weighted and then filled in the flume. After packing the soil to a design depth (0.3, 0.6, 0.9 and 1.2 m), a watering pot was used to spray the soil surface until surface runoff was generated. Then the plot was covered with a plastic sheet to prevent soil moisture evaporation and allowed to stand for 24 h. In this study, it took 20 days from the completion of soil loading to the start of the experiment. The same amount of sprayed water (10 L) was carried out in each filled soil flume at a 5-days interval for a total of 4 times. The sprayed operation can prevent the filled topsoil in the flume from drying out quickly, produce better cohesion between the soil layers, and also ensure the similar initial soil moisture among different soil flumes. After 20 days of soil filling in flume, the measured soil bulk density, organic matter content and stable infiltration rate in the soil flume are 1.36–1.56 g cm^{-3}, 0.47–1.03% and 0.24–0.61 mm min^{-1}, respectively, which is basically close to that of the investigated undisturbed soil.

Given the fact that approximately 63% of the total runoff volume is generated from upstream flat drainage area (0–5°) and this runoff can initiate gully headcut erosion that contributes 86.3% of the total soil loss in the loess-tableland and gully area of the Loess Plateau (Guo et al., 2019), we can judge that the upstream area is the landscape position that mainly provides the most of runoff causing gully headcut erosion and only contributes little soil loss. Therefore, we generalized the upstream area as a thin soil layer that was not eroded by water. As a result, a 0.01 m non-erodible soil surface layer with 1.35 g cm^{-3} soil bulk density was designed and placed on the filling soil layers to ensure that the sediment concentrate of upstream flows passed the edge of headwall was close to zero and then transformed to jet flow and on-wall flow. This treatment also can ensure the separation of the flow upstream gully head is only controlled by experimental conditions (flow discharges and headwall heights). The non-erodible layer consisted of a 5–2 mixture of soil and cement according to the method proposed by Wells et al. (2013) and Qin et al. (2018). The non-erodible layer was subjected to a 15 mm h^{-1} rainfall until the surface runoff and little-puddles occurred (about 30 min), and then a fan was employed to force air over surface for curing the non-erodible layer.

2.3. Device installation for the separation and measurement of jet flow and on-wall flow

This study includes three sub-experiments: jet flow experiment (JF), on-wall flow experiment (OF) and the mixed flow experiment (jet flow and on-wall flow are not separated, MF) for completing our study objectives. The JF means the on-wall flow was separated from the flow at headwall position to study the effects of jet flow (Fig. 2a). The OF means the jet flow was separated from the flow at the edge of headwall to investigate the effects of on-wall flow (Fig. 2b).

For the JF, a 'U' shaped steel-flume was embedded in the headwall soil to collect on-wall flow (Fig. 2a). Three fine steel needles were embedded in the headwall soil at the bottom of the 'U' shaped flume to stabilize the flume. The inside depth, outside depth, width of the flume and the width embedding into headwall are 5 cm, 4 cm, 3 cm and 2 cm, respectively (Fig. 2a). The left and right ends of the flume are 2 cm and 10 cm away from the edge of headwall, which can ensure the slope of 3° between the flume and horizontal level to drain away the separated on-wall flow. The area between flume and the edge of headwall was also set as the non-erodible layer to prevent on-wall flow from eroding headwall soil. Another flume with same size was installed along the plot boundary-wall to drain the separated on-wall flow into the sampling bucket (Fig. 2a). Simultaneously, the separated jet flow scoured the gully-bed, and then the runoff and sediment process at the bottom of gully-bed was monitored and collected by using sampling buckets. This treatment can ensure that the on-wall flow can be completely collected without affecting the erosion process of jet flow, so it is highly consistent with the real ground situation.

For the OF, a rectangular flow-collected flume and its steel support frame were firstly installed in front of headwall. The spacing between headwall and the flow-collected flume kept at a short distance (approximately 3–5 cm) to ensure that the flow-collected flume did not affect the on-wall flow scouring headwall soils and also can collect all separated jet flow. The dimension of the rectangular flow-collected separated flume is 1.48 m (width) × 0.5 m (length) × 0.2 m (depth), and another rectangular flow-drained flume with 10 cm × 10 cm of width and depth was welded in the center of flow-collected flume for draining the separated jet flow. The height of steel support frame could be adjusted from 0.3 m to 0.9 m for the experiments of different headwall heights. The sampling buckets were also placed under the bottom of gully-bed and flow drained flume to monitor runoff and sediment process and the varied process of jet flow discharge, respectively.

The MF means that no any device was installed to separate the flow from upstream area. The implementation of MF under same experimental conditions with JF and OF is to detect the effects of the interaction of jet flow and on-wall flow on soil loss and the effects of on-wall flow on plunge pool morphology.

2.4. Experimental procedure

Before the formal experiments, the flow discharge was firstly adjusted to the five designed flow discharge. A water supply system consisting of a pump, pipes, valve groups, an electromagnetic flowmeter and a pressure gauge was used to supply water for the flow-steady pool of the experimental flume. The designed flow discharges can be obtained by adjusting valve groups and monitoring with electromagnetic flowmeter in the water supply system. The clear water after energy dissipation by the water-drop structure in the flow-steady pool overflowed gradually the flow-steady pool and then entered the upstream area. The flow velocity apparatus (LS300-A, relative error less than 1.5%) was employed to measure the flow velocity at the edge of headwall (V_j) and the flow velocity outside of the plunge pool (V_p) with 5–8 times at 2-minute interval. Meanwhile, the flow depth and width at upstream area and gully-bed were measured by using a steel rule (1 mm accuracy). During the JF and OF experiments, the on-wall flow discharge and jet flow discharge were monitored by sampling buckets, respectively; and for the three sub-experiments, the runoff and sediment samples at the bottom of gully bed were collected by sampling buckets at 2-minute intervals. The

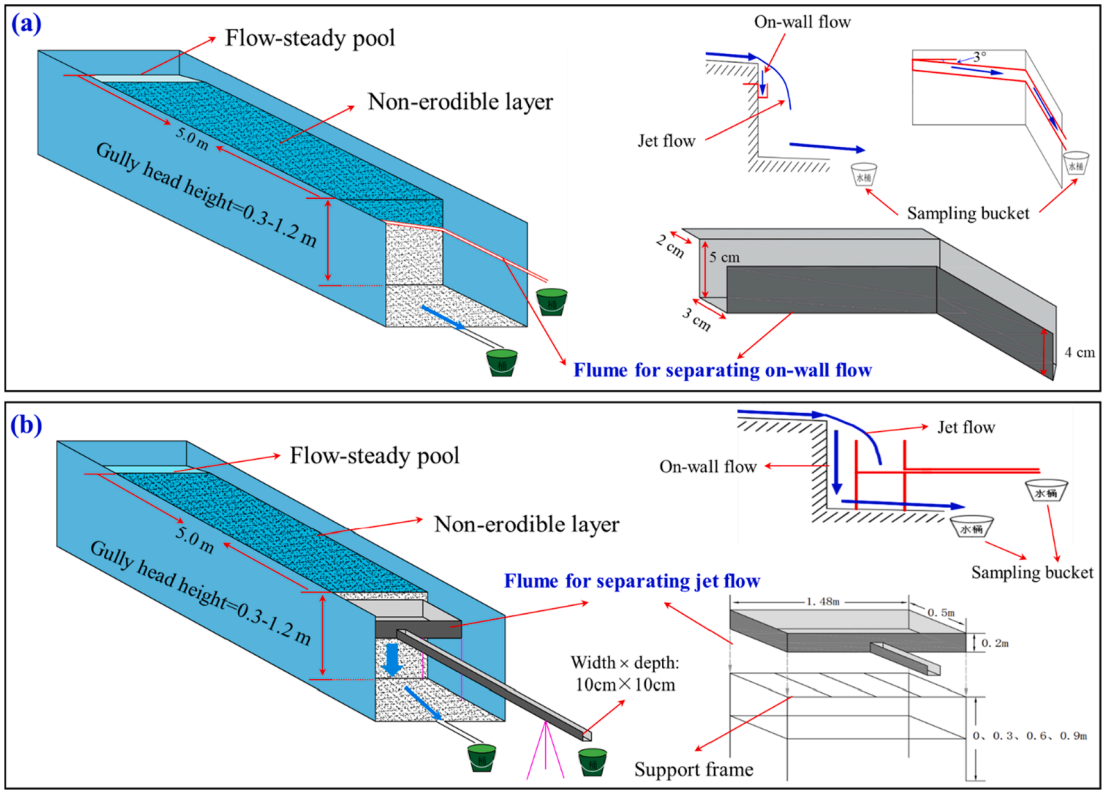

Fig. 2. Sketch of experimental plots for jet flow erosion (a) and on-wall flow erosion (b).

runoff and sediment samples were weighed and dried in an oven at 110 °C for 24-h, then reweighed for calculating soil loss rate. For JF and MF experiments, the plunge pool developed at the gully bed due to jet flow erosion, and the width (W) and depth (D) of plunge pool were measured using the steel rule with 1 mm accuracy at 2-minute intervals during experiments. The water temperature was captured during experiments at 2-minute intervals to calculate water viscosity coefficient (υ). A total of 60 experiments (3 treatments × 4 headwall heights × 5 flow discharges) were conducted in this study.

2.5. Parameter calculation

The parameters describing jet flow properties include jet flow velocity at the brink of headcut (V_b), flow velocity entry to plunge pool (V_e), jet entry angle (θ_e), and jet shear stress (τ_j), and they are calculated according to previous studies as following (Alonso et al., 2002; Zhang et al., 2016). The sketch for illustrating jet flow property parameters at headcut and plunge pool was shown in Fig. 3.

$$V_b = \begin{cases} \dfrac{\sqrt[3]{q_0 g}}{0.715}, Fr < 1 \\ V_j \cdot \dfrac{Fr^2 + 0.4}{Fr^2}, Fr > 1 \end{cases} \quad (3)$$

$$Fr = \frac{V_j}{\sqrt{g \cdot d_b}} \quad (4)$$

$$V_e = \frac{V_b}{cos\theta_e} \quad (5)$$

$$\theta_e = \arctan\left(\frac{\sqrt{2g \cdot D_H}}{V_b}\right) \quad (6)$$

$$\tau_j = 0.025(\upsilon/q_0)^{0.2} \cdot \rho_w \cdot (2g \cdot H + V_b^2) \quad (7)$$

where q_0 is the flow discharge ($m^3\ s^{-1}$); g is the gravitational acceleration ($m\ s^{-2}$); Fr is the flow Froude number; d_b is the flow depth at the brink of headcut (m); D_H is the vertical distance between brink of headcut and bottom of plunge pool (m); $H = H_0 + d_b/2$, H_0 is the initial gully head height (m); υ is the water viscosity coefficient ($m^2\ s^{-1}$).

The energy consumption of jet flow (ΔE_j, $J\ s^{-1}$) was calculated as following:

$$\Delta E_j = E_j - E_o \quad (8)$$

$$E_j = \rho_w \cdot g \cdot q_0 \cdot (L_g \cdot tan\theta + H) + \frac{1}{2}\rho_w \cdot q_0 \cdot V_b^2 \quad (9)$$

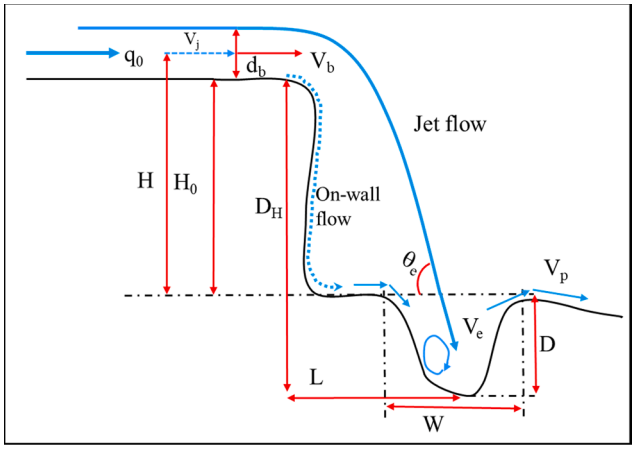

Fig. 3. Sketch of plunge pool of gully head.

$$E_o = \rho_w \cdot g \cdot q_0 \cdot \left(L_g - V_b\sqrt{\frac{2H_0}{g}}\right) \cdot tan\theta + \frac{1}{2}\rho_w \cdot q_j \cdot V_p^2 \quad (10)$$

$$q_j = \alpha \cdot q_0 \quad (11)$$

where E_j ($J\ s^{-1}$) and E_0 ($J\ s^{-1}$) is the flow energy at the brink of headcut and outside of plunge pool, respectively; ρ_w ($kg\ m^{-3}$) is the water density; L_g (m)is the projected length of gully-bed; θ (°) is the bed slope steepness; q_j is the jet flow discharge ($m^3\ s^{-1}$); α is the proportion of jet flow during JF and OF experiments and listed in Table 1.

2.6. Data analysis and figure plotting

The linear and non-linear regression analysis was employed to determine the relationships among flow discharge, gully head height, jet flow properties, soil loss amount, and plunge pool morphology. The Pearson correlation analysis was used to analyze the correlations among plunge pool morphology and jet flow properties. The extended Fourier amplitude sensitivity test (Extend FAST) was employed to calculate the sensitivity index (SI) of flow discharge (q_0) and headwall height (H_0) by using the 'fast99' function in the R package "Sensitivity" (Saltelli et al. 1999), which can judge which factor (flow discharge or gully head height) is more sensitive to soil loss amount and plunge pool dimension by jet flow, on-wall flow and their interaction. The data statistical analysis was carried out in SPSS software (version 16.0) and R software (version 3.6.3). The figure plotting was conducted by using Origin software (version 2020), Adobe Illustrator CC (version 2018) and PowerPoint software (version 2016).

3. Results

3.1. Proportion of jet flow and on-wall flow

Table 1 shows the volume and proportion of jet flow and on-wall flow under JF and OF experiments with different flow discharge and gully head height conditions. The volume and proportion of on-wall flow under JF experiment condition were 0.9%–10.9% and 0.07%–10.1% times higher than those under OF experiment condition, respectively. On average, the differences in the volume and proportion between JF and OF experiments was less 5%, indicating the JF and OF experiments were reliable in the study for separating jet flow and on-wall flow. Under the same flow discharge condition, the difference in jet flow or on-wall flow volume was small among different gully head heights, indicating the gully head height slightly affected the proportions of jet flow and on-wall flow. The on-wall flow volume (V_o) ranged from 330 to 563 L and linearly increased with the increasing flow discharge ($R^2 = 0.996$, $P < 0.01$), but the proportion of on-wall flow (P_o, 15.7%–22.6%) to the total flow volume decreased with the flow discharge as a power function ($R^2 = 0.996$, $P < 0.01$). The volume (V_j) and proportion (P_j) of jet flow were 1131–3014 L and 77.43%-84.27%, respectively, which increased with the flow discharge as a linear and logarithmic function, respectively ($R^2 = 0.992$–0.999, $P < 0.01$).

3.2. Contributions of jet flow and on-wall flow to soil loss

Fig. 4 illustrates the changes in soil loss amount caused by jet flow, on-wall flow and the interaction of jet flow and on-wall flow with flow discharge under different gully head height conditions. For the JF experiments (Fig. 4a), the soil loss amount caused by jet flow (SY_j) increased with flow discharge as two power functions for gully head height of 0.3 m and 1.2 m, but it linearly increased with flow discharge increasing under 0.6 m and 0.9 m gully head heights (Table 2). Furthermore, the SY_j increased with gully head height as two power functions for the flow discharge of 3.0 and 3.6 $m^3\ h^{-1}$, but it increased exponentially with gully head height for the other flow discharges

Table 1
Volume and proportion of jet flow and on-wall flow under different flow discharge and gully head height conditions.

H_0 (m)	q_0 (m^3 h^{-1})	OF				JF			
		V_o (L)	V_j (L)	P_o	P_j	V_o (L)	V_j (L)	P_o	P_j
0.3	3.0	312	1178	20.9%	79.1%	343	1145	23.0%	77.0%
	3.6	345	1428	19.5%	80.5%	377	1421	21.0%	79.1%
	4.8	420	1959	17.7%	82.3%	446	1923	18.8%	81.2%
	6.0	487	2477	16.4%	83.6%	526	2441	17.7%	82.3%
	7.2	546	3046	15.2%	84.8%	571	3010	15.9%	84.1%
0.6	3.0	333	1148	22.5%	77.5%	327	1100	22.9%	77.1%
	3.6	340	1429	19.2%	80.8%	367	1433	20.4%	79.6%
	4.8	422	1948	17.8%	82.2%	426	1875	18.5%	81.5%
	6.0	502	2483	16.8%	83.2%	507	2458	17.1%	82.9%
	7.2	559	3050	15.5%	84.5%	581	3004	16.2%	83.8%
0.9	3.0	337	1132	22.9%	77.1%	343	1114	23.5%	76.5%
	3.6	389	1409	21.6%	78.4%	385	1338	22.4%	77.7%
	4.8	430	1944	18.1%	81.9%	452	1921	19.1%	80.9%
	6.0	508	2427	17.3%	82.7%	521	2453	17.5%	82.5%
	7.2	577	3020	16.0%	84.0%	568	2993	16.0%	84.0%
1.2	3.0	320	1108	22.4%	77.6%	324	1121	22.4%	77.6%
	3.6	383	1393	21.6%	78.4%	363	1415	20.4%	79.6%
	4.8	444	1971	18.4%	81.6%	448	1906	19.0%	81.0%
	6.0	511	2474	17.1%	82.9%	525	2413	17.9%	82.1%
	7.2	522	3000	14.8%	85.2%	579	2988	16.2%	83.8%

Note: OF, on-wall flow experiment; JF, jet flow experiment; H_0, initial gully head height; q_0, flow discharge; V_o, on-wall flow volume; V_j, jet flow volume; P_o, the proportion of on-wall flow; P_j, the proportion of jet flow.

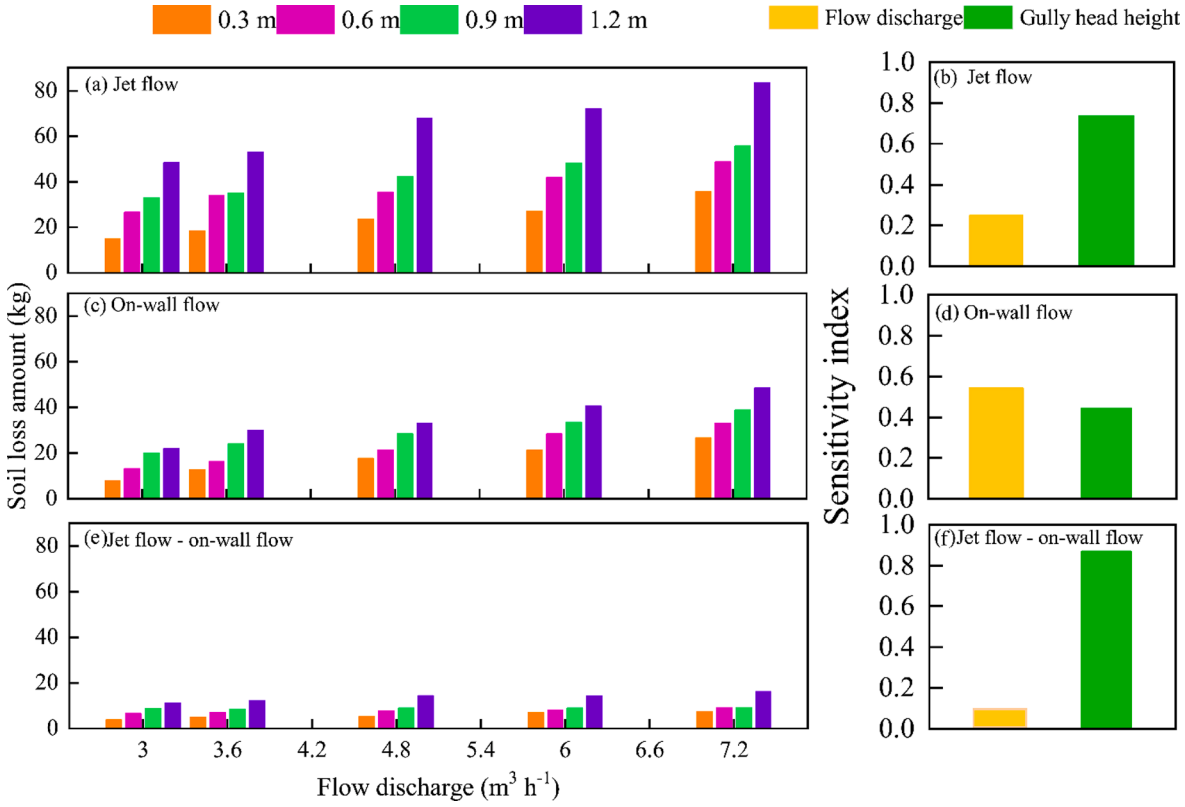

Fig. 4. Soil loss amount caused by jet flow, on-wall flow and their interaction and their sensitivity to flow discharge and gully head height.

(Table 3). Consequently, an empirical model (Eq. (12)) involving flow discharge (q_0) and gully head height (H_0) could estimate SY_j well with the high coefficient of determination (0.966). Furthermore, the extended Fourier amplitude sensitivity test (Extend FAST) showed the sensitivity index of q_0 and H_0 is 0.25 and 0.73, indicating that H_0 is the more sensitive factor affecting soil loss caused by jet flow than q_0 (Fig. 4b).

Similarly, for the OF experiments (Fig. 4c), the soil loss amount caused by on-wall flow (SY_o) increased by 0.82–1.76 times when gully head height increased from 0.3 m to 1.2 m, and the power, linear and exponential functions could express the relationship between SY_o and gully head height (Table 3). With the increase of flow discharge, the on-wall flow volume also increased (Table 1), and it also caused the increase of SY_o. When the gully head height is 0.3 m and 1.2 m, the SY_o logarithmically and linearly increased with flow discharge, respectively, but it increased with flow discharge as two power functions for 0.6 m and 0.9 m gully head heights (Table 2). Like the SY_j, the SY_o also could be expressed by the Eq. (13) with a same form of Eq. (12). The extend

Table 2
Relationships between soil loss caused by jet-flow, on-wall flow and their interaction and flow discharge under different gully head height conditions.

H_0 / (m)	SY_j	SY_o	SY_{inter}
0.3	$SY_j = 5.36q_0^{0.94}$, $R^2 = 0.986^{**}$	$SY_o = 20.27\ln(q_0) - 14.07$, $R^2 = 0.991^{**}$	$SY_{inter} = 3.92\ln(q_0) - 0.39$, $R^2 = 0.946^{**}$
0.6	$SY_j = 4.74q_0 + 14.03$, $R^2 = 0.949^{**}$	$SY_o = 4.13q_0^{1.06}$, $R^2 = 0.997^{**}$	$SY_{inter} = 2.68\ln(q_0) + 3.53$, $R^2 = 0.985^{**}$
0.9	$SY_j = 5.46q_0 + 15.97$, $R^2 = 0.997^{**}$	$SY_o = 9.20q_0^{0.73}$, $R^2 = 0.995^{**}$	—
1.2	$SY_j = 24.37q_0^{0.62}$, $R^2 = 0.983^{**}$	$SY_o = 5.84q_0 + 6.07$, $R^2 = 0.970^{**}$	$SY_{inter} = 5.40\ln(q_0) + 5.24$, $R^2 = 0.949^{**}$

Note: the H_0, SY_j, SY_o, and SY_{inter} refers to gully head height, soil loss amount caused by jet flow, on-wall flow and the interaction of jet flow and on-wall flow, respectively. The ** indicates the significant level of 0.01. The sampling number is 5 for fitting equations.

Table 3
Relationships between soil loss induced by jet-flow, on-wall flow and their interaction and gully head height under different flow discharge conditions.

q_0 / (m^3/h)	SY_j	SY_o	SY_{inter}
3.0	$SY_j = 39.27H_0^{0.81}$, $R^2 = 0.983^{**}$	$SY_o = 20.02H_0^{0.77}$, $R^2 = 0.985^{**}$	$SY_{inter} = 9.59H_0^{0.77}$, $R^2 = 0.999^{**}$
3.6	$SY_j = 43.80H_0^{0.71}$, $R^2 = 0.933^{*}$	$SY_o = 9.29\exp(0.99H_0)$, $R^2 = 0.990^{**}$	$SY_{inter} = 3.83\exp(0.94H_0)$, $R^2 = 0.989^{**}$
4.8	$SY_j = 17.12\exp(1.11H_0)$, $R^2 = 0.974^{**}$	$SY_o = 14.08\exp(0.73H_0)$, $R^2 = 0.987^{**}$	$SY_{inter} = 3.87\exp(1.05H_0)$, $R^2 = 0.964^{**}$
6.0	$SY_j = 20.60\exp(1.03H_0)$, $R^2 = 0.968^{**}$	$SY_o = 20.94H_0 + 15.21$, $R^2 = 0.996^{**}$	—
7.2	$SY_J = 27.24\exp(0.90H_0)$, $R^2 = 0.967^{**}$	$SY_o = 22.02\exp(0.65H_0)$, $R^2 = 0.995^{**}$	—

Note: the q_0, SY_j, SY_o, and SY_{inter} refer to flow discharge, soil loss amount caused by jet flow, on-wall flow and the interaction of jet flow and on-wall flow, respectively. The * and ** indicate the significant level of 0.05 and 0.01, respectively. The sampling number is 4 for fitting equations.

FAST indicated that the q_0 had slightly larger effect on SY_o than H_0 (Fig. 4d). Further, by comparing the parameters in the two equations, we found the sensitive of SY_o to flow discharge was higher than SY_j, but the gully head height showed a higher effect on SY_j than SY_o.

Fig. 4e shows the change of soil loss amount caused by the interaction of jet flow and on-wall flow (SY_{inter}) with flow discharge and gully head height. Regression analysis showed the SY_{inter} logarithmically increased with flow discharge except for 0.9 m gully head height (R^2 = 0.946–0.985). Under the same flow discharge condition, the SY_{inter} increased by 1.09–1.93 times with the gully head height increasing from 0.3 m to 1.2 m. However, only when flow discharge is less than 6.0 m^3 h^{-1}, the SY_{inter} is a significant power or exponential function of gully head height. Furthermore, the SY_{inter} can be estimated by a composite function of flow discharge and gully head height (Eq. (14)). However, the extend FAST found that the SY_{inter} showed a weak sensitivity to q_0 and was mainly affected by H_0 (Fig. 4f)

$$SY_j = 6.623q_0^{0.643}\hat{A}\cdot\exp(1.041H_0), R^2 = 0.966, P < 0.01, N = 20 \quad (12)$$

$$SY_o = 3.615q_0^{0.876}\hat{A}\cdot\exp(0.732H_0), R^2 = 0.974, P < 0.01, N = 20 \quad (13)$$

$$SY_{inter} = 0.865(1.554lnq_0 + 2.283)\hat{A}\cdot\exp(0.982H_0), R^2 = 0.926, P < 0.01, N = 20 \quad (14)$$

Fig. 5 shows the change in the contributions of jet flow, on-wall flow and the interaction of jet flow and on-wall flow to total soil loss under different flow discharge and gully head height conditions. The proportion of soil loss by jet flow to total soil loss (P_j) was 49.1%–56.1%, 53.4%–59.4%, 51.9%–53.8%, 55.8%–59.5%, respectively, under 0.3 m, 0.6 m, 0.9 m, and 1.2 m gully head height condition. The P_j showed a relatively small change with flow discharge increasing, and it also fluctuated with gully head height increasing. The proportion of soil loss by on-wall flow to total soil loss (P_o) ranged from 26.9% to 38.6% in this study. Similarly, the P_o also fluctuated with the increase of gully head height, but it logarithmically increased with flow discharge ($P_o = a\cdot ln(q_0) + b$, a = 5.07 – 10.73, b = 15.95 – 28.04, R^2 = 0.771–0.939). The proportion of soil loss by the interaction of jet flow and on-wall flow to total soil loss (P_{inter}) accounted for 9.9%-14.2% of total soil loss. The P_{inter} logarithmically decreased with flow discharge ($P_{inter} = c\cdot ln(q_0) + d$, c = − 3.07 – 5.97, d = 16.92 – 20.54, R^2 = 0.789 – 0.993) but showed a relatively small change among different gully head heights. Under our experimental conditions, the P_j: P_o: P_{inter} ranged from 4: 3: 1 to 4.4: 2 :1 with the averaged ratio of 4.6: 3 :1, implying that the jet flow contributed the most of soil loss, and the interaction of jet flow and on-wall flow only caused the 11.6% of the total soil loss.

3.3. Plunge pool morphology

3.3.1. Plunge pool width

Fig. 6 shows the similar evolution process of plunge pool width (W_j) by jet flow among different gully head height and flow discharge conditions. Overall, the W_j rapidly increased in the initial 8 min and then gradually increased to a stable state after 24 min. Several fluctuates occurred during the evolution of plunge pool, which was mainly attributed to the situation that the headwall soil was eroded and then deposited around the plunge pool. With the development of plunge pool, the dynamic balance between soil detachment and sediment transport occurred, implying that the morphology of plunge pool would keep a relatively stable state. Further analysis showed the temporal change in W_j could be expressed by a series of logarithmic functions (Table 4, R2 = 0.889 – 0.994). However, the temporal change of the plunge pool width by jet flow and on-wall flow (W_m) showed the stronger fluctuation than that by jet flow (Fig. 6). Especially, for the experiment under 1.2 m gully head height, the W_m exhibited a drastic fluctuation during 10–20 min. This phenomenon could be explained by the fact that the eroded soil from gully headwall by on-wall flow was imported into plunge pool and then affected jet flow erosion process, especially, the headwall failure would form a sudden effect on plunge pool. After 24 min, the width of plunge pool gradually stabilized. In most cases, the W_m increased logarithmically with experimental time (Table 4, R2 = 0.379–0.962). In comparison, the greater R^2 was found in W_j than W_m (Table 4), further indicating the on-wall flow erosion process does affect the evolution process of plunge pool width.

After 30-min experiment concluded, with the low flow discharge increasing from 3.0 to 7.2 m^3 h^{-1}, the W_j gradually increased from low values of 23.4, 24.7, 27.0 and 31.0 cm to high values of 31.0, 38.0, 40.7 and 44.3 cm, under gully head height of 0.3, 0.6, 0.9 and 1.2 m, respectively (Fig. 7). For each gully head height, the W_j increased exponentially with the increase of flow discharge ($W_j = a\cdot\exp(b\cdot q_0)$, a = 18.73–24.79, b = 0.070–0.093, R^2 = 0.889–0.990). Under the flow discharge of 3.0, 3.6, and 4.8 m^3 h^{-1}, the W_j increased exponentially with the increase of gully head height (R^2 = 0.884–0.961), but it increased logarithmically with the increase of gully head height under 6.0 and 7.2 m^3 h^{-1} (R^2 = 0.995 and 0.993). For the MF experiments, the plunge pool width (W_m) ranged from 10.0 to 46.0 cm, and it exponentially increased with flow discharge ($W_m = a\cdot\exp(b\cdot q_0)$, a = 7.91–17.79, b = 0.099–0.16, R^2 = 0.919–0.991), as well as the gully head height ($W_m = a\cdot\exp(b\cdot H_0)$, a = 6.79–11.44, b = 0.94–1.14, R^2 = 0.926–0.992). Non-linear regression analysis showed that the W_j and W_m could be estimated by two composite functions of flow discharge and gully head height (Eqs. (15) and (16)). Furthermore, the extend FAST showed that

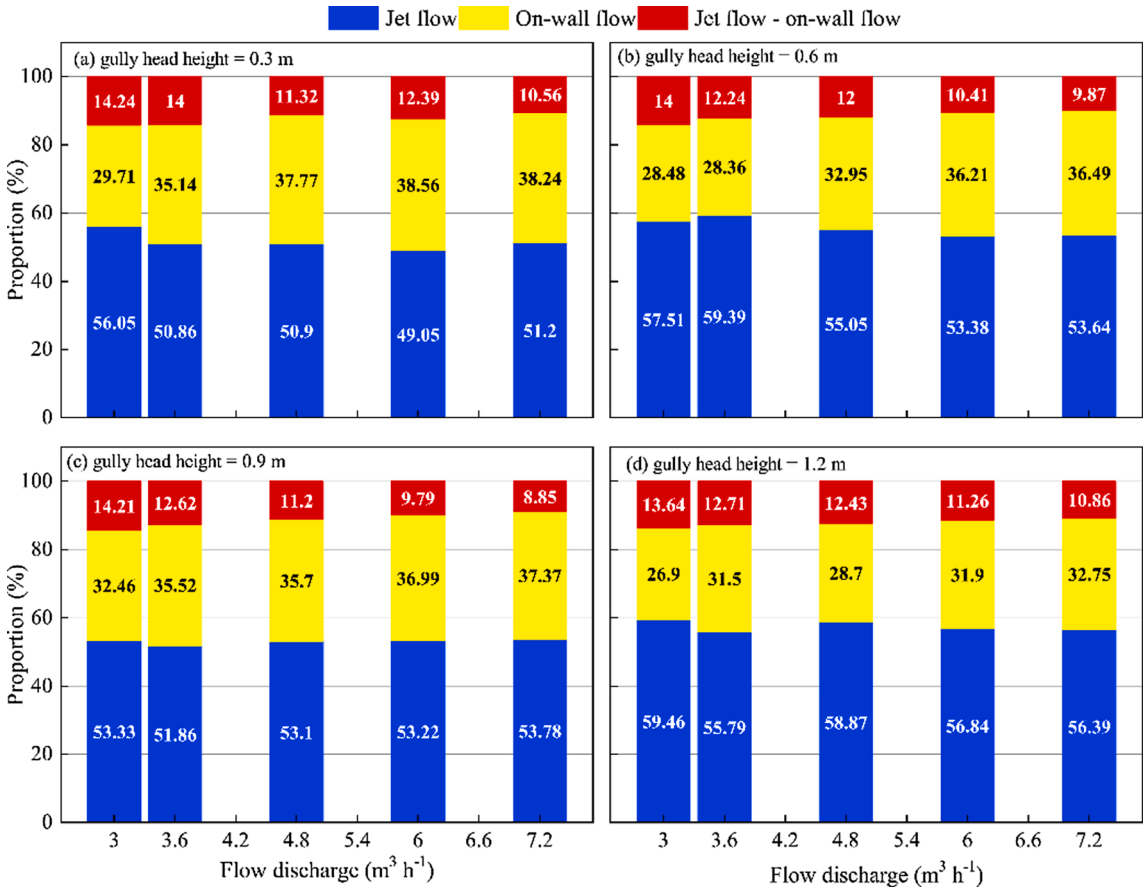

Fig. 5. Proportions of soil loss amount induced by jet flow, on-wall flow and their interaction.

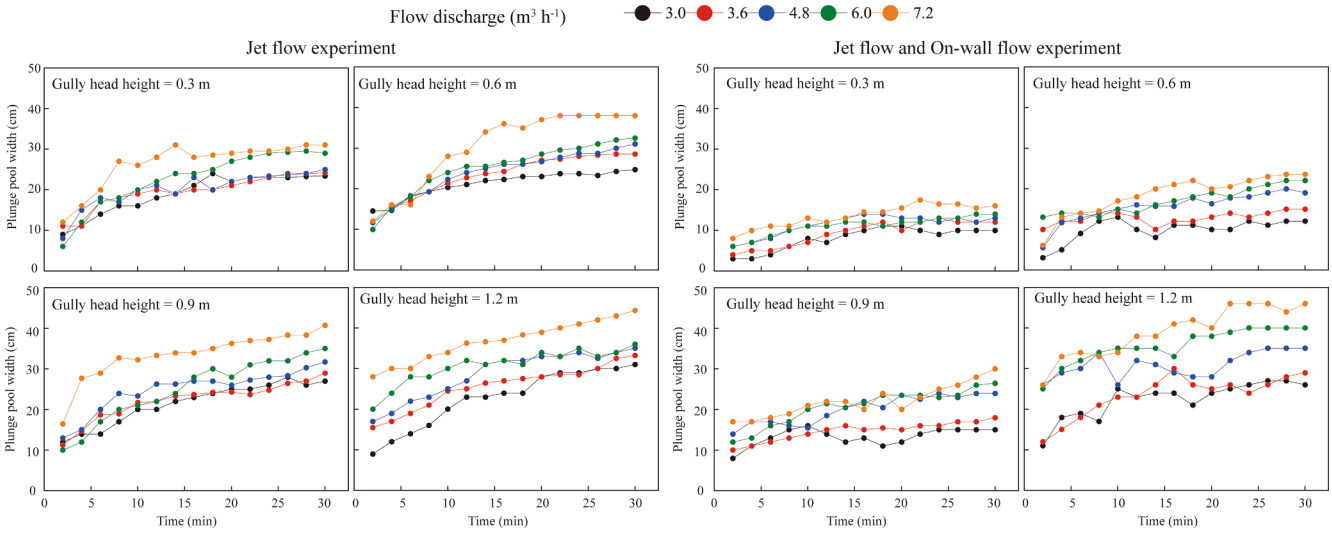

Fig. 6. Evolution process of plunge pool width under different flow discharge and gully head height conditions.

the *SI* of q_0 and H_0 is 0.38 and 0.62, respectively under JF condition, and it is 0.75 and 0.23, respectively under MF condition, which indicating that H_0 had the greater effect on the plunge pool width, but q_0 showed a greater effect under MF condition.

$$W_j = 22.43\hat{A}\cdot H_0^{0.212}\hat{A}\cdot\exp(0.084q_0), R^2 = 0.954, P < 0.01 \quad (15)$$

$$W_m = 4.509\hat{A}\cdot\exp(1.129H_0 + 0.134q_0), R^2 = 0.975, P < 0.01 \quad (16)$$

The difference in plunge pool width between JF and MF experiments was compared to clear the effect of on-wall flow (Fig. 7). The plunge pool width caused by the combination of jet flow and on-wall flow were 48.0%-57.3%, 32.3%-51.4%, and 24.3%-44.4% less than those caused by jet flow under gully head height of 0.3, 0.6 and 0.9 m, respectively, and the difference decreased with the increase of flow discharge, indicating the effect of on-wall flow on plunge pool width gradually decreased with the flow discharge increased. Notably, when gully head height is 1.2 m and flow discharge is larger than 4.8 $m^3\ h^{-1}$, the plunge

Table 4
Relationships between plunge pool width and time under different flow discharge and gully head height conditions.

H_0 (m)	q_0 (m^3 h^{-1})	JF Fitted equation	R^2	MF Fitted equation	R^2
0.3	3.0	$W_j = 6.07\ln(t) + 3.54$	0.952**	$W_m = 3.32\ln(t)$-0.41	0.851**
	3.6	$W_j = 5.08\ln(t) + 6.57$	0.932**	$W_m = 3.74\ln(t)$-0.22	0.885**
	4.8	$W_j = 6.38\ln(t) + 5.39$	0.916**	$W_m = 2.92\ln(t) + 3.95$	0.813**
	6.0	$W_j = 8.87\ln(t)$-0.01	0.992**	$W_m = 2.94\ln(t) + 3.59$	0.948**
	7.2	$W_j = 6.98\ln(t) + 8.62$	0.889**	$W_m = 3.37\ln(t) + 5.03$	0.902**
0.6	3.0	$W_j = 4.10\ln(t) + 10.72$	0.967**	$W_m = 2.75\ln(t) + 2.92$	0.604**
	3.6	$W_j = 7.12\ln(t) + 4.98$	0.994**	$W_P = 1.22\ln(t) + 9.75$	0.379*
	4.8	$W_j = 7.20\ln(t) + 5.65$	0.988**	$W_P = 4.53\ln(t) + 4.03$	0.945**
	6.0	$W_j = 8.19\ln(t) + 4.25$	0.992**	$W_m = 0.35\ t + 11.50$	0.937**
	7.2	$W_j = 11.54\ln(t) + 0.95$	0.939**	$W_m = 6.13\ln(t) + 2.88$	0.962**
0.9	3.0	$W_j = 6.42\ln(t) + 5.14$	0.944**	$W_m = 1.77\ln(t) + 8.76$	0.411*
	3.6	$W_j = 5.88\ln(t) + 7.25$	0.966**	$W_m = 0.24\ t + 10.86$	0.874**
	4.8	$W_j = 6.49\ln(t) + 8.34$	0.940**	$W_m = 0.37\ t + 14.28$	0.871**
	6.0	$W_j = 9.85\ln(t)$-0.09	0.959**	$W_m = 0.46\ t + 13.35$	0.881**
	7.2	$W_j = 7.23\ln(t) + 15.04$	0.932**	$W_m = 0.40\ t + 15.71$	0.846**
1.2	3.0	$W_j = 8.96\ln(t)$-0.08	0.960**	$W_m = 5.26\ln(t) + 9.03$	0.841**
	3.6	$W_j = 6.63\ln(t) + 8.66$	0.949**	$W_m = 6.02\ln(t) + 8.08$	0.859**
	4.8	$W_j = 7.43\ln(t) + 9.65$	0.948**	$W_m = 0.23\ t + 27.19$	0.423*
	6.0	$W_j = 5.33\ln(t) + 17.13$	0.946**	$W_m = 5.38\ln(t) + 21.87$	0.925**
	7.2	$W_j = 6.16\ln(t) + 21.11$	0.930**	$W_m = 7.46\ln(t) + 20.09$	0.903**

Note: H_0, q_0, JF and MF refer to the gully head height, flow discharge, jet flow experiment and jet flow and on-wall flow experiment, respectively. W_j and W_m indicate the plunge pool width caused by jet flow and the interaction of jet flow and on-wall flow, respectively. The * and ** indicate the significant level of 0.05 and 0.01, respectively. The sampling number is 15 for fitting equations.

pool width under MF was larger than that under JF, indicating the presence of on-wall flow promoted the development of plunge pool width and increased it by 7.5% on average.

3.3.2. Plunge pool depth

The temporal change in the plunge pool depth (D) under JF and MF conditions is shown in the Fig. 8. For the JF experiments, overall, the depth by jet flow (D_j) rapidly increased in the first 10 min and then trended to stable state. However, for the MF experiments under same conditions with JF, the developed process of plunge pool depth (D_m) showed the stronger fluctuation than JF experiments. Moreover, the larger flow discharge and gully head height intensified the fluctuation of change process of plunge pool depth. In fact, without the effect of on-wall flow erosion on plunge pool, the dynamic change of plunge pool depth was mainly depended on the dynamic change in energy consumption of jet flow in plunge pool. With the increase of plunge pool depth, the energy consumption of jet flow also increased gradually, and the depth would stabilize when the energy consumption reaches to the extremum. However, for the MF experiments, the development of plunge pool was also affected by on-wall flow erosion. The soil loss of gully headwall caused by on-wall flow and splashed water drops from plunge pool would enter into plunge pool and further change the energy consumption process of jet flow in plunge pool, and the random soil failures of gully head also aggravated the fluctuation degree in the developmental process of plunge pool depth. For the 90% of cases, the temporal variation in D_j and D_m could be expressed by a series of logarithmic functions (Table 5, R2 = 0.345–0.970), and, judged from the values of the coefficient of determination (R^2), the D_m showed the relatively weaker relationships with time than D_j due to the effects of on-wall flow erosion.

After 30-min JF experiment concluded, with the flow discharge increased from 3.0 to 7.2 m^3 h^{-1}, the D_j increased from the lowest values of 14, 15.2, 16.5 and 19 cm to the highest values of 20, 22.3, 26 and 28 cm, when the gully headwall height is 0.3, 0.6, 0.9 and 1.2 m, respectively (Fig. 9). For each head height, the relationship between D_j and flow discharge can be expressed by an exponential function ($D_j = a{\cdot}\exp(b{\cdot}q_0)$, a = 11.05–15.16, b = 0.082–0.11, R^2 = 0.890–0.986), and, similarly, a series exponential functions also can reveal the relationship between D_j and gully headwall height ($D_j = a{\cdot}\exp(b{\cdot}H_0)$, a = 12.52–17.85, b = 0.33–0.42, R^2 = 0.944–0.995). However, for the MF experiments, the existence of on-wall flow erosion not only impeded the development of plunge pool depth (4–20 cm), but also changed the relationships between D_m and flow discharge to logarithmic functions ($D_m = a{\cdot}\ln(q_0) + b$, a = 7.06–12.31, b = −4.58–3.57, R^2 = 0.959–0.995), and, with the increase of gully headwall height, the increment of D_m gradually decreased for each flow discharge. Further analysis indicated that the D_j and D_m could be estimated by two composite functions of flow discharge and gully headwall height (Eqs. (17) and (18)). Furthermore, the greater SI (0.54) of H_0 than that (0.46) of q_0 under JF condition indicated that the headwall height had the stronger impact on depth. However, the on-wall flow erosion completely changed this situation and the SI of q_0 and H_0 is 0.83 and 0.15, respectively, fully indicating the q_0 mainly dominated the development of plunge pool depth under MF condition.

$$D_j = 9.721\hat{A}{\cdot}\exp(0.379H_0 + 0.088q_0), R^2 = 0.960, P < 0.01 \quad (17)$$

$$D_m = 1.535q_0^{0.688}\hat{A}{\cdot}(1.085lnH_0 + 3.184), R^2 = 0.943, P < 0.01 \quad (18)$$

The D_m were reduced by 40.0%–71.4%, 31.0%-44.7%, 27.8%–33.5% and 28.6%-52.6% compared to D_j, when gully headwall height is 0.3, 0.6, 0.9 and 1.2 m, respectively, and the decrease in plunge pool depth decreased with the flow discharge increased, indicating that larger flow discharge would weaken the effect of on-wall flow erosion on the development of plunge pool depth, which was basically consistent with the effect of on-wall flow on plunge pool width (Fig. 7). In addition, we found the ratio of width to depth ranged from 1.38 to 1.70 with the average value of 1.57 under jet flow condition, but it increased to 1.33–2.89 with an average of 1.79 due to the presence of on-wall flow erosion, which also further indicated that the effect of on-wall flow erosion on the development of plunge pool depth was higher than the width.

3.4. Relationships plunge pool morphology and jet flow properties

For the JF and MF experiments, the plunge pool width and depth showed the significant correlation with jet properties except for jet flow velocity at the brink of headcut ($P < 0.01$, Table 6), of which the energy consumption of jet flow showed the strongest correlation with plunge pool morphology, followed by jet shear stress, flow velocity entry to plunge pool and jet entry angle. This also further indicated energy consumption of jet flow is a determined factor influencing the development of plunge pool morphology during headcut erosion. Regression analysis revealed that the W_j and W_m linearly increased with the increase of energy consumption (Fig. 10a, $P < 0.01$). Notably, the slope of fitted line (1.637) under MF was nearly 2 times that under JF, and the W_m would excess W_j when energy consumption is larger than 21.90 J

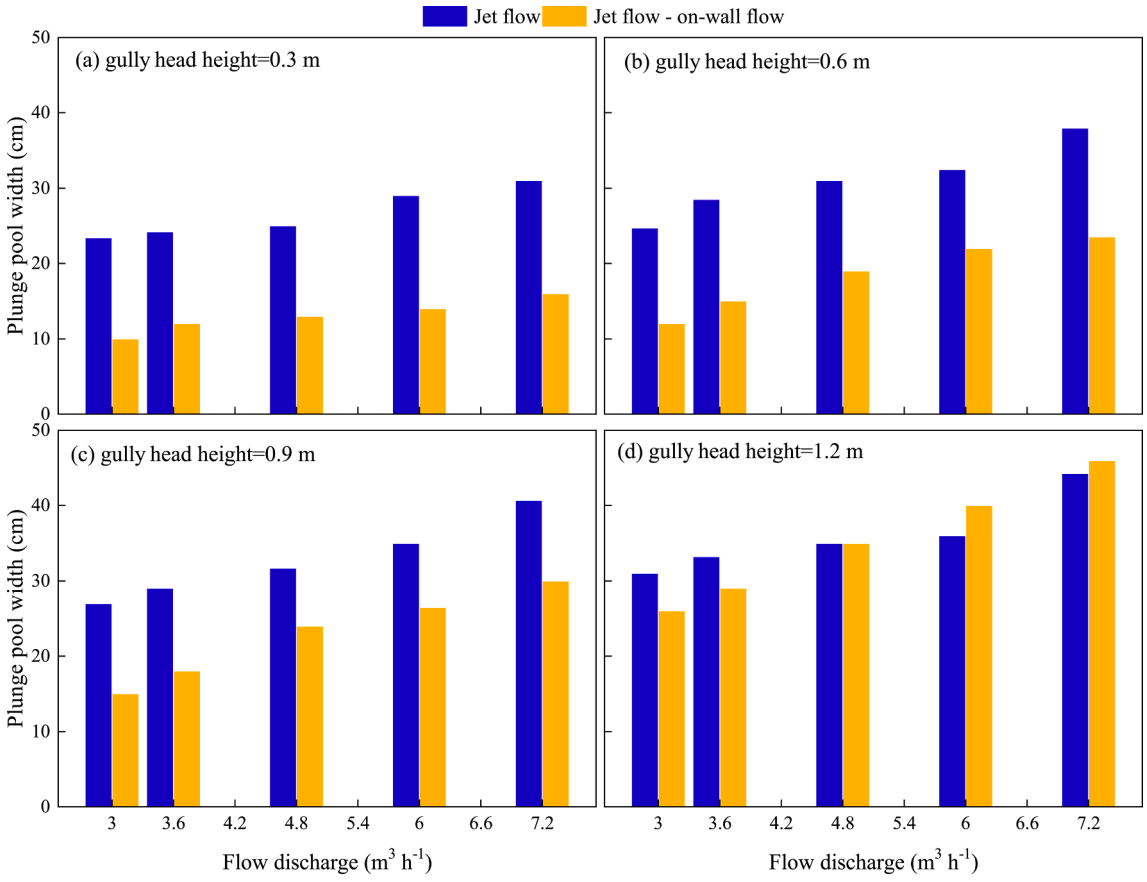

Fig. 7. Difference of plunge pool width between jet flow and jet flow – on-wall flow experiments.

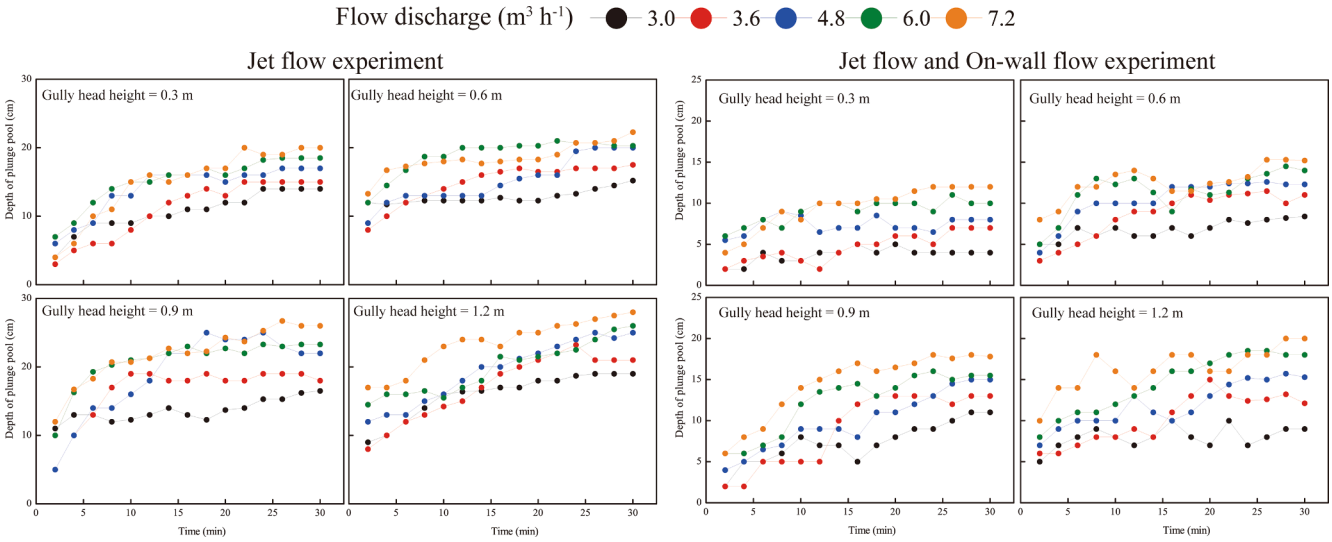

Fig. 8. Evolution process of plunge pool depth under jet flow and on-wall flow experimental conditions.

s^{-1}, implying the presence of on-wall accelerated the development of plunge pool width. In addition, the D_j also linearly increased with the increase of energy consumption, but D_m increased with energy consumption by a power function (Fig. 10b), which indicated that the D_j would always be greater than D_m under same energy consumption and also cleared the fact that the on-wall flow erosion could greatly weakened the effect of energy consumption of jet flow on the development of plunge pool depth.

4. Discussion

Our result showed that the on-wall flow volume linearly increased with the increasing flow discharge, and its proportion to the total flow volume (15.7%–22.6%) decreased with the flow discharge as a power function. However, the volume and proportion of jet flow increased with the flow discharge as a linear and logarithmic function, respectively. This was basically consistent with the conclusion of Chen et al. (2013) who studied the effect of jet flow and on-wall flow on collapse of gully

Table 5
Relationships between plunge pool depth and time under jet flow and jet flow - on-wall flow experimental conditions.

H_0 / (m)	q_0 / (m^3/h)	JF Fitted equation	R^2	MF Fitted equation	R^2
0.3	3.0	$D_j = 3.56\ln(t) + 1.57$	0.942**	$D_m = 0.87\ln(t) + 1.51$	0.591**
	3.6	$D_j = 5.29\ln(t)$-2.50	0.928**	$D_m = 1.84\ln(t)$-0.08	0.690**
	4.8	$D_j = 4.36\ln(t) + 2.94$	0.910**	—	—
	6.0	$D_j = 4.36\ln(t) + 4.06$	0.970**	$D_m = 1.63\ln(t) + 4.89$	0.791**
	7.2	$D_j = 6.37\ln(t)$-1.26	0.964**	$D_m = 3.20\ln(t) + 1.41$	0.962**
0.6	3.0	$D_j = 0.10\ t + 11.23$	0.760**	$D_m = 0.11\ t + 5.12$	0.731**
	3.6	$D_j = 3.65\ln(t) + 5.55$	0.968**	$D_m = 3.49\ln(t)$-0.25	0.930**
	4.8	$D_j = 3.87\ln(t) + 5.29$	0.789**	$D_m = 3.15\ln(t) + 2.43$	0.937**
	6.0	$D_j = 3.15\ln(t) + 10.91$	0.90**	$D_m = 2.66\ln(t) + 4.59$	0.629**
	7.2	$D_j = 2.48\ln(t) + 12.15$	0.820**	$D_m = 2.23\ln(t) + 6.87$	0.688**
0.9	3.0	$D_j = 0.16\ t + 11.15$	0.765**	$D_m = 2.84\ln(t) + 0.08$	0.792**
	3.6	$D_j = 4.66\ln(t) + 4.69$	0.790**	$D_m = 5.20\ln(t)$-4.22	0.837**
	4.8	$D_j = 7.34\ln(t) + 0.33$	0.903**	$D_m = 4.20\ln(t)$-0.78	0.864**
	6.0	$D_j = 4.24\ln(t) + 10.03$	0.874**	$D_m = 4.43\ln(t) + 1.06$	0.882**
	7.2	$D_j = 4.97\ln(t) + 9.22$	0.965**	$D_m = 4.93\ln(t) + 1.95$	0.955**
1.2	3.0	$D_j = 4.12\ln(t) + 5.47$	0.969**	$D_m = 0.98\ln(t) + 5.49$	0.345*
	3.6	$D_j = 5.91\ln(t) + 2.08$	0.925**	$D_m = 3.32\ln(t) + 1.82$	0.760**
	4.8	$D_j = 5.64\ln(t) + 5.01$	0.909**	$D_m = 3.08\ln(t) + 4.11$	0.784**
	6.0	$D_j = 0.42\ t + 13.18$	0.944**	$D_m = 4.34\ln(t) + 3.51$	0.923**
	7.2	$D_j = 4.52\ln(t) + 11.90$	0.927**	$D_m = 2.86\ln(t) + 9.10$	0.718**

Note: H_0, q_0, JF and MF refer to the gully headwall height, flow discharge, jet flow experiment and jet flow and on-wall flow experiment, respectively. D_j and D_m indicate the plunge pool depth caused by jet flow and the interaction of jet flow and on-wall flow, respectively. The * and ** indicate the significant level of 0.05 and 0.01, respectively. The sampling number is 15 for fitting equations.

heads under real ground situations and found the P_o also decreased with flow discharge increasing, fully demonstrating that our experimental results are consistent with the changing law of the proportions of jet flow and on-wall flow under real ground condition and so this result can be used for reference as a basis for the size design of gully head protection engineering measures. Furthermore, we found that, in their studies, the P_o can reach up to 56.8% when flow discharge was less than 0.25 m^3 h^{-1}, which is much larger than the results of this study. However, the P_o decreased from 26.3% to 9.3% when flow discharge increased from 0.51 to 2.5 m^3 h^{-1}, portending that the lower flow discharge could cause similar P_o with our study. This difference was mainly related to the flow discharge and hydraulic properties (Dias and Tuck, 1991; Wiryanto, 1999; Dias and Vanden-Broeck, 2011). Peng et al. (2012) concluded that the Froude number (*Fr*) is equal to 0.015 and the Reynold number is equal to 9500 are the critical conditions initiating the transformation of on-wall flow to jet flow. However, Dias and Tuck (1991) stated that the turbulent degree of the flow is the main factor influencing the formation of the jet flow and on-wall flow. The on-wall flow is easy to form at the gully head when *Fr* is less than 1, and the jet flow would become the main flow type when *Fr* is larger than 1. In addition, the soil properties also affect the water-soil interface tension and the runoff hydraulic characteristics, and thus were expected to change the proportions of jet flow and on-wall flow (Wang, 2002; Peng et al., 2012).

The formation of headcut generally derived from the step change in underlying surface elevation, and it divides the concentrated flow into on-wall flow and jet flow (Poesen et al., 2003; Guo et al., 2019). The occurrence and migration of headcuts and the change in concentrated flow properties commonly lead to the obvious increase in soil loss (Römkens et al., 1997; Alonso et al., 2002). However, the sediment contributions of on-wall flow and jet flow are not clear and not explicitly addressed in some gully erosion models (Renard et al., 1991; Nearing et al., 1989; Stein et al., 1993; Alonso et al., 2002; Zhao et al., 2013). Our study distinguished firstly and preliminarily the soil loss amounts caused by jet flow, on-wall flow and their interaction from total soil loss and found that the soil loss amount increased significantly with the increase of q_0 and H_0 (Fig. 3), which deepened the understanding of the role of jet flow and on-wall flow in controlling gully erosion. The further analysis showed that the soil loss by jet flow had the higher sensitivity to H_0 than q_0, and the soil loss of on-wall flow showed the opposite result, fully indicating that the two critical influencing factors exhibited different effects on different sub-processes of gully headcut erosion (Vanmaercke et al., 2016). Furthermore, on average, the jet flow, on-wall flow and their interaction can contribute 53.5%, 34.9% and 11.6% of total soil loss amount, respectively, which demonstrated that jet flow erosion contributed more than half of soil loss amount. This is mainly because more than 70% of the flow volume upstream gully head is converted into jet flow (Table 1), which means that more energy of jet flow is consumed in soil detachment and transportation from plunge pool erosion (Zhang et al., 2018). In addition, we found that the larger flow discharge significantly improved the sediment contributions of on-wall flow and but decreased the contribution of the interaction of jet flow and on-wall flow. This is mainly due to the situation that the larger flow discharge caused the developed position of plunge pool away from headwall, and thus the water drops from plunge pool only caused little effect on headwall erosion by on-wall flow. These results fully reveals that the serious gully erosion is mainly attributed to the fact that the gully head separated the concentrated flow as the jet flow and on-wall flow which not only dominated the different sub-processes of gully erosion but also contributes more soil loss than concentrated flow erosion (Valentin et al., 2005). Therefore, it is necessary to pay attention to how to deal with the jet flow and on-wall flow reasonably in the process of gully erosion prevention and control. Our study revealed that the rapid growth in the depth and width of plunge pool occurred in the 10-min initial period, and then the dimensions of plunge pool developed slowly. Similar results were also found in some published works on rill and bank gully headcut erosion (e.g., Stein et al., 1993; Bennett and Casalí, 2001; Zhang et al., 2016). For example, Stein et al. (1993) stated a more detailed result that the rate of plunge pool scour depth increased rapidly when the scour depth was less than 95% of the equilibrium depth. Furthermore, in most of cases, it was found that the plunge pool morphology (width and depth) increased logarithmically with experimental duration (Tables 4, 5). This result was supported by Rouse (1940) who suggested that the sour depth increased linearly with the log of the time. However, Blaisdell et al. (1981) confirmed the hyperbolic function has a computable scour depth and gives the best fit, but unfortunately, the scour depth may be reached the equilibrium only after extremely long times. As a result, the semi-log relationship between scour depth and time was popularly preferred by many researchers (Rajaratnam, 1981; Alonso et al., 2002; Wells et al., 2009a, 2010; Campo-Bescós et al., 2013), although it indicated that the scour depth increased infinitely with time in a physical sense. Notably, the plunge pool morphology retained a steady constant at the end of experiments (Figs. 5, 7), which was consistent with previous studies on rill and bank gully headcut erosion (e.g., Bennett, 1999; Bennett et al., 2000; Wells et al., 2009a, 2009b; Zhang et al., 2016) and also further indicated that the development of plunge pool morphology entered into an equilibrium phase when the scour hole eroded to the point that the maximum jet

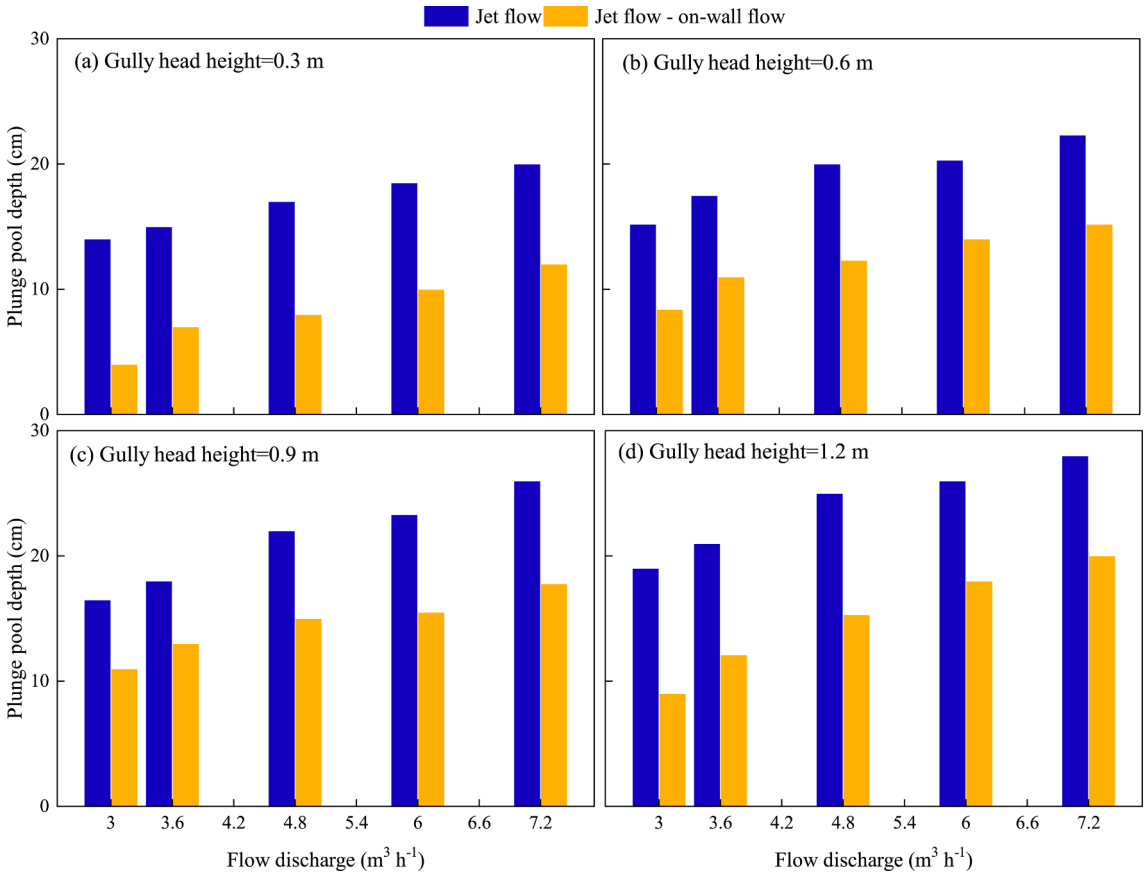

Fig. 9. Difference in plunge pool depth between jet flow and jet flow – on-wall flow experiments.

Table 6
Correlations between plunge pool width and depth and jet flow properties.

Experiment type	Variable	Jet flow velocity at the brink of headcut	Flow velocity entry to plunge pool	Jet entry angle	Jet shear stress	Energy consumption of jet flow
JF	W_j	0.313 ^{ns}	0.672**	0.644**	0.680**	0.925**
	D_j	0.390 ^{ns}	0.717**	0.651**	0.726**	0.955**
MF	W_m	−0.052 ^{ns}	0.853**	0.728**	0.868**	0.97**
	D_m	0.285 ^{ns}	0.696**	0.697**	0.699**	0.921**

Note: JF, jet flow experiment; MF, the combined experiment of jet flow and on-wall flow; W_j and D_j were the width and depth of plunge pool under JF, respectively; W_m and D_m were the width and depth of plunge pool under MF. The sample number is 20. ** refers to the significant level of 0.01, and ns refers to significant level of greater than 0.05.

shear stress of the diffused jet equals the critical shear stress of the gully bed soil (a balance between the jet eroding forces and soil resistances) (Alonso et al., 2002). However, in some cases, the obvious fluctuation was found during the development of plunge pool morphology under MF experiments (Figs. 5, 7), implying that the presence of on-wall flow erosion altered the evolution process of plunge pool morphology. This was mainly attributed to the random headwall soil failure induced by on-wall flow suddenly filling into the pool (Zhang et al., 2016; Guo et al., 2019; Shi et al., 2020).

The narrower and deeper plunge pool (width: 10–46 cm, depth: 4–28 cm) was developed in this study than those (width: 64.2–80.1 cm, depth: 5.6–8.1 cm) in the study of Zhang et al. (2016), although the flow discharge and headwall height condition is similar between the two studies. The difference was mainly caused by the difference in gully bed material. The higher soil bulk density (1.73 g cm^{-3}) and clay content (27%) in the study of Zhang et al. (2016) than this study signified the lower soil erodibility and higher erosion resistance to jet flow (Guo et al., 2018, 2020), and thus the quicker lateral development of plunge pool is found in their study than this study. In addition, the final plunge pool morphology increased significantly with the increase of q_0 and H_0 (Eq. (4–7)), which was agreed with some previous studies (e.g., Bennett et al., 2000; Alonso et al., 2002; Zhang et al., 2016; Guo et al., 2019). This result was also supported by a realistic theory predictive model involving mainly the unit flow discharge, gully head height, flow velocity at the brink-point and gully-bed materials, of which the q_0 and H_0 is the main factors controlling the plunge pool erosion (Alonso et al., 2002). The initial flow discharge and headwall height determined the jet properties entering plunge pool. Our result showed that the jet property parameters (except for the jet flow velocity at the brink of headcut) significantly influenced the development of plunge pool morphology, of which the energy consumption of jet flow had the strongest correlation with plunge pool morphology and could be considered as the critical factor predicting plunge pool erosion. Several studies on gully and bank gully headcut erosion also obtained a similar conclusion (e.g., Su et al., 2014; Zhang et al., 2018; Shi et al., 2020). The great difference in the relationships between plunge pool morphology and energy consumption between JF and MF conditions (Fig. 9) indicated that the on-wall flow erosion would weaken the effect of energy consumption on scour depth

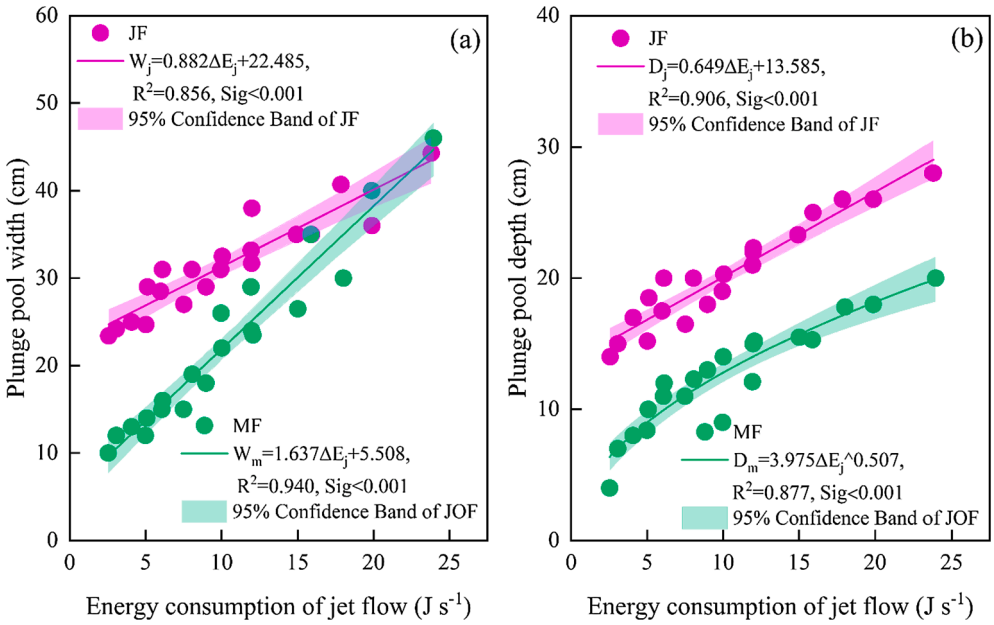

Fig. 10. The relationships between plunge pool morphology and energy consumption of jet flow. Note: JF and MF refer to the jet flow experiment and jet flow and on-wall flow experiment, respectively. W_j and W_m are the width of plunge pool under JF and MF experiment, respectively. D_j and D_m are the plunge pool depth under JF and MF experiment, respectively.

but improve the effect on plunge pool width. Moreover, the on-wall flow erosion changed the sensitivity of plunge pool evolution to H_0 and q_0, and under real ground situation, the concentrated flow discharge upstream gully head exhibited the stronger effects on plunge pool morphology than headwall height. Therefore, the future study should consider how to regulate the concentrated flow in drainage area upstream gully heads to weaken gully erosion.

5. Limitations and significance of this study

Despite nearly a century of gully erosion studies, gully erosion remains a poorly understand processes and dynamic mechanism, which is important for the modelling and prediction of gully erosion and its prevention and control. Our study separated the jet flow and on-wall flow through a series of simulated flow experiments combined with a self-made separated device and clarified their influences on soil loss of gully heads and the morphological evolution of plunge pool. However, there are two potential limitations: (1) the experimental design of this study was idealized and generated due to the complex effects of lots of factors on gully erosion, so it is not on the same scale as the actual situations; (2) it has not been confirmed how well the experimental results are in line with the actual ground results. Therefore, further studies need to optimize the experimental design and verify the experimental results with the actual situations, so that the study results can be practiced and applied under actual conditions. Although the earlier-noted imperfection represents the limitation of our study, we still clearly demonstrated the ratio of jet flow and on-wall flow volume to total flow volume upstream gully head, and further clarified their influences on soil loss of gully heads and morphological development of plunge pool during gully erosion process, which is of great significance for deepening the understanding of the gully process and mechanism. Moreover, to a certain extent, it can also provide scientific basis for the establishment of process-based gully erosion model and the design of gully erosion prevention measures.

6. Conclusion

This study explored the proportion of jet flow and on-wall flow and their influences on soil loss and plunge pool morphology during headcut erosion. The proportion of on-wall flow and jet flow is 15.7% – 22.6% and 77.4% – 84.3% of total flow, respectively. The jet flow erosion contributed the highest proportion of total soil loss (53.5%), followed by on-wall flow (34.9%) and their interaction (11.6%). The soil loss caused by jet flow and its interaction with on-wall flow was dominated by H_0, but q_0 had the greater effect on soil loss caused by on-wall flow than H_0. The width and depth of plunge pool logarithmically increased under jet flow and the combination of jet flow and on-wall flow condition. The dimension of plunge pool was significantly enhanced by flow discharge and headwall height. The on-wall flow erosion weakened the plunge pool depth by 27.8% – 71.4%. Similarly, the width was reduced by 24.3%–57.3% under headwall height of 0.3–0.9 m, but the on-wall flow promoted plunge pool width by 7.5% when H_0 is 1.2 m and q_0 is larger than 4.8 m^3 h^{-1}. The on-wall flow erosion can change the sensitivity of plunge pool evolution to H_0 and q_0, and the concentrated flow upstream gully head exhibited the stronger effects on plunge pool morphology under real ground situation. The energy consumption of jet flow showed the strongest effect on the evolution of plunge pool morphology. This study elucidated the importance role of jet flow and on-wall flow in controlling gully headcut erosion and deepened the understanding of gully erosion processes and mechanism.

CRediT authorship contribution statement

Mingming Guo: Conceptualization, Data curation, Formal analysis, Investigation, Methodology, Resources, Validation, Visualization, Writing - original draft, Writing - review & editing. **Yibao Lou:** Conceptualization, Data curation, Formal analysis, Investigation, Resources, Visualization, Writing - original draft. **Zhuoxin Chen:** Data curation, Formal analysis, Methodology, Software, Writing - original draft. **Wenlong Wang:** Conceptualization, Funding acquisition, Methodology, Project administration, Resources, Supervision, Validation, Visualization, Writing - review & editing. **Lanqian Feng:** Data curation, Formal analysis, Investigation, Methodology. **Xingyi Zhang:** Conceptualization, Formal analysis, Methodology, Resources, Validation.

Declaration of Competing Interest

The authors declare that they have no known competing financial

interests or personal relationships that could have appeared to influence the work reported in this paper.

Acknowledgements

Financial support for this work was provided by the National Natural Science Foundation of China [grant number 42077079] and the China Postdoctoral Science Foundation [grant number 2020M681062].

References

Alonso, C.V., Bennett, S.J., Stein, O.R., 2002. Predicting head cut erosion and migration in concentrated flows typical of upland areas. Water Resour. Res. 38 (12), 39-1–39-15. https://doi.org/10.1029/2001WR001173.

Bennett, S.J., 1999. Effect of slope on the growth and migration of headcuts in rills. Geomorphology 30 (3), 273–290. https://doi.org/10.1016/S0169-555X(99)00035-5.

Bennett, S.J., Casalí, J., 2001. Effect of initial step height on headcut development in upland concentrated flows. Water Resour. Res. 37 (5), 1475–1484. https://doi.org/10.1029/2000WR900373.

Bennett, S.J., Alonso, C.V., Prasad, S.N., Römkens, M.J.M., 2000. Experiments on headcut growth and migration in concentrated flows typical of upland areas. Water Resour. Res. 36 (7), 1911–1922. https://doi.org/10.1029/2000WR900067.

Blaisdell, F.W., Anderson, C.L., Hebaus, G.G., 1981. Ultimate dimensions of local scour. J. Hydraul. Div. ASCE 107 (3), 327–337. https://doi.org/10.1243/03093247V164251.

Campo-Bescós, M.A., Flores-Cervantes, J.H., Bras, R.L., Casalí, J., Giráldez, J.V., 2013. Evaluation of a gully headcut retreat model using multitemporal aerial photographs and digital elevation models. J. Geophys. Res. Earth Surf. 118 (4), 2159–2173. https://doi.org/10.1002/jgrf.20147.

Cheng, H., Wu, Y., Zou, X., Si, H.a., Zhao, Y., Liu, D., Yue, X., 2006. Study of ephemeral gully erosion in a small upland catchment on the Inner-Mongolian Plateau. Soil Till. Res. 90 (1-2), 184–193. https://doi.org/10.1016/j.still.2005.09.006.

Collison, A.J.C., 2001. The cycle of instability: stress release and fissure flow as controls on gully head retreat. Hydrol. Process. 15 (1), 3–12. https://doi.org/10.1002/(ISSN)1099-108510.1002/hyp.v15:110.1002/hyp.150.

De Ploey, J., 1989. A model for headcut retreat in gullies. Catena 14, 81–86.

Dias, F., Tuck, E.O., 1991. Weir flows and waterfalls. J. Fluid Mech. 230, 525–539. https://doi.org/10.1017/S0022112091000885.

Dias, F., Vanden-Broeck, J.M., 2011. Potential-flow studies of steady two-dimensional jets, waterfalls, weirs and sprays. J. Eng. Math. 70 (1–3), 165–174. https://doi.org/10.1007/s10665-010-9441-5.

Gómez-Gutiérrez, Á., Schnabel, S., Berenguer-Sempere, F., Lavado-Contador, F., Rubio-Delgado, J., 2014. Using 3D photo-reconstruction methods to estimate gully headcut erosion. Catena 120, 91–101. https://doi.org/10.1016/j.catena.2014.04.004.

Guo, M., Wang, W., Shi, Q., Chen, T., Kang, H., Li, J., 2019. An experimental study on the effects of grass root density on gully headcut erosion in the gully region of China's Loess Plateau. Land Degrad. Dev. 30 (17), 2107–2125. https://doi.org/10.1002/ldr.v30.1710.1002/ldr.3404.

Guo, M.M., Wang, W.L., Kang, H.L., Yang, B., 2018. Changes in soil properties and erodibility of gully heads induced by vegetation restoration on the Loess Plateau, China. J. Arid Land 10 (5), 712–725. https://doi.org/10.1007/s40333-018-0121-z.

Guo, M., Wang, W., Wang, T., Wang, W., Kang, H., 2020. Impacts of different vegetation restoration options on gully head soil resistance and soil erosion in loess tablelands. Earth Surface Process. Landforms 45 (4), 1038–1050. https://doi.org/10.1002/esp.v45.410.1002/esp.4798.

Hanson, G.J., Robinson, K.M., Cook, K.R., 2001. Prediction of headcut migration using a deterministic approach. Trans. ASAE 44 (3), 525–531. https://doi.org/10.13031/2013.6112.

Heckmann, T., Cavalli, M., Cerdan, O., Foersterd, S., Javauxe, M., Lodef, E., Smetanovág, A., Vericath, D., Brardinoni, F., 2018. Indices of sediment connectivity: Opportunities, challenges and limitations. Earth Sci. Rev. 187, 77–108. https://doi.org/10.1016/j.earscirev.2018.08.004.

Ionita, I., 2006. Gully development in the Moldavian Plateau of Romania. Catena 68, 133–140. https://doi.org/10.1016/j.catena.2006.04.008.

Li, H., Cruse, R.M., Liu, X., Zhang, X., 2016. Effects of topography and land use change on gully development in typical Mollisol Region of Northeast China. Chin. Geogra. Sci. 26 (6), 779–788. https://doi.org/10.1007/s11769-016-0837-7.

Li, M., Song, X.Y., Shen, B., Li, H.Y., Meng, C.X., 2006. Influence of vegetation change on producing runoff and sediment in gully region of Loess Plateau. J. Northwest Sci-Tech. Univer. Agric. Forest. (Natural Science Edition) 34 (1), 117–120. https://doi.org/10.13207/j.cnki.jnwafu.2006.01.025.

Liu, H., Zhang, T., Liu, B., Liu, G., Wilson, G.V., 2013. Effects of gully erosion and gully filling on soil depth and crop production in the black soil region, northeast China. Environ. Earth Sci. 68 (6), 1723–1732. https://doi.org/10.1007/s12665-012-1863-0.

Moeyersons, J., Makanzu Imwangana, F., Dewitte, O., 2015. Site-and rainfall-specific runoff coefficients and mega-gully development in Kinshasa (DR Congo). Nat. Hazards 79, 203–233. https://doi.org/10.1007/s11069-015-1870-z.

Nearing, M.A., Foster, G.R., Lane, L.J., Finkner, S.C., 1989. A process based soil erosion model for USDA—Water erosion prediction project technology. Trans. ASAE 32, 1587–1593. https://doi.org/10.13031/2013.31195.

Oostwoud Wijdenes, D., Poesen, J., Vandekerckhove, L., Ghesquiere, M., 2000. Spatial distribution of gully head activity and sediment supply along an ephemeral channel in a Mediterranean environment. Catena 39 (3), 147–167. https://doi.org/10.1016/S0341-8162(99)00092-2.

Oostwoud Wijdenes, D.J., Bryan, R., 2001. Gully-head erosion processes on a semi-arid valley floor in Kenya: a case study into temporal variation and sediment budgeting. Earth Surf. Process. Landf. 26 (9), 911–933. https://doi.org/10.1002/esp.v26:910.1002/esp.225.

Peng, R.W., Zhang, X., Peng, Y.H., 2012. Experimental research on hydraulic characteristics of wall pressing flow for rectangle sharp-crested weir. J. North China Inst. Water Conserv. Hydroelectric Power 33 (3), 23–26 (In Chinese).

Poesen, J., Nachtergaele, J., Verstraeten, G., Valentin, C., 2003. Gully erosion and environmental change: Importance and research needs. Catena 50 (2–4), 91–133. https://doi.org/10.1016/S0341-8162(02)00143-1.

Prasad, S.N., Römkens, M.J.M., 2003. Energy formulations of head cut dynamics. Catena 50 (2-4), 469–487. https://doi.org/10.1016/S0341-8162(02)00125-X.

Qin, C., Zheng, F., Wells, R.R., Xu, X., Wang, B., Zhong, K., 2018. A laboratory study of channel sidewall expansion in upland concentrated flows. Soil Till. Res. 178, 22–31. https://doi.org/10.1016/j.still.2017.12.008.

Rajaratnam, N., 1981. Erosion by plane turbulent jets. J. Hydr. Res. 19 (4), 339–359. https://doi.org/10.1080/00221688109499508.

Renard, K.G., Foster, G.R., Weesies, G.A., Porter, J.P., 1991. RUSLE: revised universal soil loss equation. J. Soil Water Conserv. 46 (1), 30–33. https://doi.org/10.1002/9781444328455.ch8.

Rengers, F.K., Tucker, G.E., 2014. Analysis and modeling of gully headcut dynamics, North American high plains. J. Geophys. Res. Earth Surf. 119 (5), 983–1003. https://doi.org/10.1002/2013JF002962.

Robinson, K.M., Hanson, G.J., 1994. A deterministic headcut advance model. Trans. ASAE 37 (5), 1437–4143. https://doi.org/10.13031/2013.28225.

Rodzik, J., Furtak, T., Zglobicki, W., 2009. The impact of snowmelt and heavy rainfall runoff on erosion rates in a gully system, Lublin Upland. Poland. Earth Surf. Process. Landf. 34 (14), 1938–1950. https://doi.org/10.1002/esp.v34:1410.1002/esp.1882.

Römkens, M.J.M., Prasad, S.N., Gerits, J.J.P., 1997. Soil erosion modes of sealing soils: A phenomenological study. Soil Tech. 11 (1), 31–41. https://doi.org/10.1016/S0933-3630(96)00113-4.

Rouse, H., 1940. In: Criteria for Similarity in the transportation of sediment, Proc, 1st Hydraulic Conf. State University of Iowa, Iowa City, Iowa, pp. 33–49.

Saltelli, A., Tarantola, S., Chan, P., 1999. A quantitative model-independent method for global sensitivity analysis of model output. Technometrics 41 (1), 39–56. https://doi.org/10.1080/00401706.1999.10485594.

Sanchis, M.P.S., Torri, D., Borselli, L., Poesen, J., 2008. Climate effects on soil erodibility. Earth Surf. Process. Landf. 33 (7), 1082–1097. https://doi.org/10.1002/(ISSN)1096-983710.1002/esp.v33:710.1002/esp.1604.

Shi, Q., Wang, W., Guo, M., Chen, Z., Feng, L., Zhao, M., Xiao, H., 2020. The impact of flow discharge on the hydraulic characteristics of headcut erosion processes in the gully region of the Loess Plateau. Hydrol. Process. 34 (3), 718–729. https://doi.org/10.1002/hyp.v34.310.1002/hyp.13620.

Stein, O.R., Alonso, C.V., Julien, P.V., 1993. Mechanics of jet scour downstream of a headcut. J. Hydraul. Eng. ASCE 31 (6), 723–738. https://doi.org/10.1080/00221689309498814.

Su, Z.A., Xiong, D.H., Dong, Y.F., Li, J.J., Yang, D., Zhang, J.H., He, G.X., 2014. Simulated headward erosion of bank gullies in the Dry-hot Valley Region of southwest China. Geomorphology 204, 532–541. https://doi.org/10.1016/j.geomorph.2013.08.033.

Temple, D., Moore, J., 1997. Headcut advance prediction for earthen spillways. Trans. ASAE 40, 557–562. https://doi.org/10.13031/2013.21314.

Torri, D., Poesen, J., 2014. A review of topographic threshold conditions for gully head development in different environments. Earth Sci. Rev. 130, 73–85. https://doi.org/10.1016/j.earscirev.2013.12.006.

Valentin, C., Poesen, J., Li, Y., 2005. Gully erosion: impacts, factors and control. Catena 63 (2-3), 132–153. https://doi.org/10.1016/j.catena.2005.06.001.

Vandekerckhove, L., Poesen, J., Oostwoud Wijdenes, D., Gyssels, G., 2001. Short-term bank gully retreat rates in Mediterranean environments. Catena 44 (2), 133–161. https://doi.org/10.1016/S0341-8162(00)00152-1.

Vanmaercke, M., Poesen, J., Van Mele, B., Demuzere, M., Bruynseels, A., Golosov, V., Bezerra, J.F.R., Bolysov, S., Dvinskih, A., Frankl, A., Fuseina, Y., Guerra, A.J.T., Haregeweyn, N., Ionita, I., Makanzu Imwangana, F., Moeyersons, J., Moshe, I., Nazari Samani, A., Niacsu, L., Nyssen, J., Otsuki, Y., Radoane, M., Rysin, I., Ryzhov, Y.V., Yermolaev, O., 2016. How fast do gully headcuts retreat? Earth Sci. Rev. 154, 336–355. https://doi.org/10.1016/j.earscirev.2016.01.009.

Vannoppen, W., Vanmaercke, M., De Baets, S., Poesen, J., 2015. A review of the mechanical effects of plant roots on concentrated flow erosion rates. Earth Sci. Rev. 150, 666–678. https://doi.org/10.1016/j.earscirev.2015.08.011.

Vanwalleghem, T., Van Den Eeckhaut, M., Poesen, J., Deckers, J., Nachtergaele, J., Van Oost, K., Slenters, C., 2003. Characteristics and controlling factors of old gullies under forest in a temperate humid climate: A case study from the Meerdaal Forest (Central Belgium). Geomorphology 56 (1-2), 15–29. https://doi.org/10.1016/S0169-555X(03)00043-6.

Wang, Z.F., 2002. Analysis of scale effect of thin-plate weir in hydraulic model test. J. Shandong Agric. Univ. 33 (4), 499–502 (In Chinese).

Wells, R.R., Momm, H.G., Rigby, J.R., Bennett, S.J., Bingner, R.L., Dabney, S.M., 2013. An empirical investigation of gully widening rates in upland concentrated flows. Catena 101, 114–121. https://doi.org/10.1016/j.catena.2012.10.004.

Wells, R.R., Bennett, S.J., Alonso, C.V., 2009a. Effect of soil texture, tailwater height, and pore-water pressure on the morphodynamics of migrating headcuts in upland

concentrated flows. Earth Surf. Process. Landf. 34 (14), 1867–1877. https://doi.org/10.1002/esp.v34:1410.1002/esp.1871.

Wells, R.R., Alonso, C.V., Bennett, S.J., 2009b. Morphodynamics of headcut development and soil erosion in upland concentrated flows. Soil Sci. Soc. Am. J. 73 (2), 521–530. https://doi.org/10.2136/sssaj2008.0007.

Wells, R.R., Bennett, S.J., Alonso, C.V., 2010. Modulation of headcut soil erosion in rills due to upstream sediment loads. Water Resour. Res. 46, W12531. https://doi.org/10.1029/2010WR009433.

Wiryanto, L.H., 1999. Zero gravity of free-surface flow over a weir. J. Math. Fundamental Sci. 31 (1), 1–4.

Wu, Y., Cheng, H., 2005. Monitoring of gully erosion on the Loess Plateau of China using a global positioning system. Catena 63 (2-3), 154–166. https://doi.org/10.1016/j.catena.2005.06.002.

Wu, Y.Q., Zheng, Q.H., Zhang, Y.G., Liu, B.Y., Cheng, H., Wang, Y.Z., 2008. Development of gullies and sediment production in the black soil region of northeast China. Geomorphology 101, 683–691. https://doi.org/10.1016/j.geomorph.2008.03.008.

Xu, J.Z., Li, H., Liu, X.B., Hu, W., Yang, Q.N., Hao, Y.F., Zhen, H.C., Zhang, X.Y., 2019. Gully erosion induced by snowmelt in northeast China: A case study. Sustainability 11 (7), 1–14. https://doi.org/10.3390/su11072088.

Zhang, B.J., Xiong, D.H., Su, Z.A., Yang, D., Dong, Y.F., Xiao, L., Zhang, S., Shi, L.T., 2016. Effects of initial step height on the headcut erosion of bank gullies: a case study using a 3D photo-reconstruction method in the dry-hot valley region of southwest China. Phys. Geogr. 37 (6), 409–429. https://doi.org/10.1080/02723646.2016.1219939.

Zhang, B., Xiong, D., Zhang, G., Zhang, S.u., Wu, H., Yang, D., Xiao, L., Dong, Y., Su, Z., Lu, X., 2018. Impacts of headcut height on flow energy, sediment yield and surface landform during bank gully erosion processes in the Yuanmou Dry-hot Valley region, southwest China. Earth Surface Process. Landf. 893 43 (10), 2271–2282. https://doi.org/10.1002/esp.v43.1010.1002/esp.4388.

Zhang, G.H., 2020. Advances and prospects for gully erosion researches. J. Soil Water Conserv. 34 (5), 1–13 (In Chinese).

Zhao, G., Visser, P.J., Peeters, P., Vrijling, J.K., 2013. Headcut migration prediction of the cohesive embankment breach. Eng. Geol. 164, 18–25. https://doi.org/10.1016/j.enggeo.2013.06.012.